J. Fluid Mech. (1994), vol. 273, pp. 1–29

Coherent structures in rotating three-dimensional turbulence

By PETER BARTELLO†, OLIVIER MÉTAIS AND MARCEL LESIEUR

LEGI - IMG, Institut National Polytechnique de Grenoble and Université Joseph Fourier, BP 53 X, 38041 Grenoble Cedex, France

(Received 2 June 1992 and in revised form 20 January 1994)

Numerical simulations investigating the formation and stability of quasi-two-dimensional coherent vortices in rotating homogeneous three-dimensional flow are described. In a numerical study of shear flows Lesieur, Yanase & Métais (1991) found that cyclones (respectively anticyclones) with $|\omega_{2D}| \sim O(2\Omega)$, where ω_{2D} is the vorticity and Ω is the rotation rate, are stabilized (respectively destabilized) by the rotation. A study of triply periodic pseudo-spectral simulations (64^3) was undertaken in order to investigate the vorticity asymmetry in homogeneous turbulence. Specifically, we examine (i) the possible three-dimensionalization of initially two-dimensional vortices and (ii) the emergence of quasi-two-dimensional structures in initially-isotropic three-dimensional turbulence. Direct numerical simulations of the Navier–Stokes equations are compared with large-eddy simulations employing a subgridscale model based on the second-order velocity structure function evaluated at the grid separation and with simulations employing hyperviscosity.

Isolated coherent two-dimensional vortices, obtained from a two-dimensional decay simulation, were superposed with a low-amplitude three-dimensional perturbation, and used to initialize the first set of simulations. With $\Omega = 0$, a three-dimensionalization of all vortices was observed. This occurred first in the small scales in conjunction with the formation of longitudinal hairpin vortices with vorticity perpendicular to that of the initial quasi-two-dimensional flow. In agreement with centrifugal stability arguments, when $2\Omega = [\omega_{2D}]_{rms}$ a rapid destabilization of anticyclones was observed to occur, whereas the initial two-dimensional cyclonic vortices persisted throughout the simulation. At larger Ω, both cyclones and anticyclones remained two-dimensional, consistent with the Taylor–Proudman theorem. A second set of simulations starting from isotropic three-dimensional fields was initialized by allowing a random velocity field to evolve ($\Omega = 0$) until maximum energy dissipation. When the simulations were continued with $2\Omega = [\boldsymbol{\omega} \cdot \boldsymbol{\Omega}]_{rms}/\Omega$, the three-dimensional flow was observed to organize into two-dimensional cyclonic vortices. At larger Ω, two-dimensional anticyclones also emerged from the initially-isotropic flow. The consequences for a variety of industrial and geophysical applications are clear. For quasi-two-dimensional eddies whose characteristic circulation times are of the order of Ω^{-1}, rotation induces a complete disruption of anticyclonic vortices, while stabilizing cyclonic ones.

---

† Present address: Recherche en prévision numérique, Service de l'Environnement Atmosphérique, Dorval (Québec), Canada H9P 1J3

1. Introduction

Given the assumption of large timescales, the Taylor–Proudman theorem predicts that solid-body rotation at rate $\boldsymbol{\Omega} = \Omega\hat{\boldsymbol{e}}_3$ ($\Omega > 0$) tends to two-dimensionalize the flow at low Rossby numbers, here defined as $R_o = [\boldsymbol{\omega} \cdot \boldsymbol{\Omega}]_{rms}/2\Omega^2$, where $\boldsymbol{\omega}$ is the vorticity. This result is valid to the lowest order in R_o for a flow of uniform density and of arbitrary depth measured in the direction parallel to $\boldsymbol{\Omega}$. This, together with the fact that large-scale geophysical flows are in shallow layers, justifies the application of quasi-two-dimensional dynamics to the latter. The picture that has emerged after 20 years of numerical simulations of two-dimensional turbulence is dominated by the emergence of isolated coherent vorticity structures (e.g. Fornberg 1977; Basdevant *et al.* 1981; McWilliams 1984, etc.). The robustness of these vortices in physical space has focused recent attention on vorticity dynamics. Since the range of excited scales in atmospheric and oceanic turbulence is large, the Rossby number also spans a wide range. Consequently, it is of interest to consider the possibility of flow two-dimensionalization, and the vorticity dynamics, from a more general rotating three-dimensional framework.

In addition to two-dimensional motion, rotating fluid flow also supports inertial waves, which are solutions to the linear equation

$$\frac{\partial \boldsymbol{\omega}}{\partial t}(\boldsymbol{r}, t) = 2\Omega \frac{\partial \boldsymbol{u}}{\partial x_3}(\boldsymbol{r}, t),$$

where $\boldsymbol{u}(\boldsymbol{r}, t)$ is the velocity. In Fourier space this becomes

$$\mathrm{i}\boldsymbol{k} \times \frac{\partial \hat{\boldsymbol{u}}}{\partial t}(\boldsymbol{k}, t) = 2\mathrm{i}\Omega k_3 \hat{\boldsymbol{u}}(\boldsymbol{k}, t),$$

where $\boldsymbol{k}$ is the wavevector. We seek the eigenvalues of the curl operator, i.e. $\mathrm{i}\boldsymbol{k} \times \hat{\boldsymbol{u}}(\boldsymbol{k}, t) = \lambda \hat{\boldsymbol{u}}(\boldsymbol{k}, t)$. The three solutions are $\lambda = 0$, which corresponds to Taylor–Proudman two-dimensionalization and $\lambda = \pm k$, which gives a pair of inertial waves satisfying $\hat{\boldsymbol{u}}(\boldsymbol{k}, t) = \hat{\boldsymbol{u}}(\boldsymbol{k}, 0) \exp \pm \mathrm{i}\sigma(\boldsymbol{k})t$, where $\sigma(\boldsymbol{k}) = 2\Omega k_3/k = 2\Omega \cos \theta_k$ and θ_k is the angle between the wavevector and the rotation axis, $\hat{\boldsymbol{e}}_3$. Surfaces of constant inertial-wave frequency are thus cones in Fourier space (see e.g. Greenspan 1969). In the low-R_o limit, the timescale separation between slow quasi-two-dimensional motion and fast three-dimensional inertial waves increases. However, in this study we are particularly interested in the interactions between these modes at initial Rossby numbers of order one.

Rotating fluids have been studied in the laboratory by Hart (1971), Kloosterziel & van Heijst (1991) and Bidokhti & Tritton (1992) for various turbulent and transitional flows. At $R_o \sim O(1)$ they noted that, whereas regions of two-dimensional cyclonic vorticity have increased stability, two-dimensional anticyclonic regions are destabilized via a rapid three-dimensionalization. Since the linear centrifugal instability of anticyclonic regions at critical Rossby numbers has been recently discussed by Kloosterziel & van Heijst (1991), Tritton (1992) and Smyth & Peltier (1994), we mention only briefly the result of Rayleigh (1916), who considered the three-dimensional stability of an isolated axisymmetric vortex to axisymmetric perturbations. Instability may occur in regions where

$$\Phi(r) = \frac{1}{r^3}\frac{\mathrm{d}}{\mathrm{d}r}[r u_\theta(r)]^2 = \frac{2}{r}\, u_\theta(r)\, \omega(r) < 0,$$

where $\Phi(r)$ is the Rayleigh discriminant, $u_\theta(r)$ is the tangential velocity and

$$\omega(r) = \frac{1}{r}\frac{\mathrm{d}}{\mathrm{d}r}[ru_\theta(r)]$$

is the vorticity (see e.g. Drazin & Reid 1981). For a rotating fluid, the same criterion can be applied in the inertial frame when $u(r) \to u(r) + \Omega r$ and $\omega(r) \to \omega(r) + 2\Omega$, yielding a stability/instability crossover for anticyclones when $\omega(r) = -2\Omega$, i.e. at $R_o \sim O(1)$. Bradshaw (1969) used reasoning analogous to that applied to the buoyancy term in studies of stratified shear flows, to describe rotating shear flows. The quantity corresponding to the gradient Richardson number was 'Ri' $= S(1+S)$, where $S = 2\Omega/\zeta$, and ζ is the mean-flow vorticity. Three-dimensional instability (i.e. 'convection') occurs when 'Ri' < 0, yielding maximum anticyclonic destabilization at $S = R_o^{-1} = 1/2$. Recent three-dimensional numerical simulations of mixing layers by Lesieur, Yanase & Métais (1991), wakes by Métais *et al.* (1992) and channel flow by Kristoffersen & Andersson (1993) have reproduced the vorticity asymmetry observed in the laboratory and predicted by the linear-stability arguments.

In rotating *homogeneous* turbulence we have neither the background shear of Bradshaw (1969) nor the limitation to axisymmetric flow of Rayleigh (1916). It is therefore instructive to consider the nonlinear evolution of vortex filaments for the case of initially quasi-two-dimensional flow (see Lesieur *et al.* 1991). The nonlinear evolution is constrained in the inviscid barotropic equations in that vortex tubes, tangent to the absolute vorticity $\boldsymbol{\omega} + 2\boldsymbol{\Omega}$, are material. At the maximum anticyclonic instability given by the linear arguments, the Rossby number is order one. In this case, the *absolute* vorticity field is dominated by intense quasi-two-dimensional cyclones interspersed with low-level three-dimensional structure. After the Rayleigh destabilization, the absolute-vorticity filaments in regions corresponding to the initial anticyclones are (i) weaker than the quasi-two-dimensional cyclonic filaments ($R_o \sim O(1)$) and (ii) highly twisted in the third dimension. A complete three-dimensional study of the effect of rotation on the mixing layer and wake has been performed by Yanase *et al.* (1993), Métais *et al.* (1992), and Flores (1993) both from a linear-stability and a numerical-simulation point of view. In the rotating wake calculation of Métais *et al.* (1992) it was found that the cyclonic side rolled up into stable quasi-two-dimensional structures. At the same time, the anticyclonic side gave rise to strong three-dimensional longitudinal alternate vortices, analogous to Görtler vortices. The calculations presented in §3 of this paper show similar longitudinal stretching of anticyclonic vorticity in the homogeneous case.

Although previous numerical simulations of homogeneous rotating turbulence by Bardina, Ferziger & Rogallo (1985), Dang & Roy (1985*a*, *b*), Roy (1986) and Teissèdre & Dang (1987) did not consider the vorticity asymmetry at $R_o \sim O(1)$, they have investigated the tendency for their initially isotropic flows to two-dimensionalize. These simulations as well as the two-point closure study of Cambon & Jacquin (1989) and the wind tunnel experiments of Jacquin *et al.* (1990), displayed a form of two-dimensionalization in that they developed anisotropy in the integral scales measured in the directions perpendicular and parallel to $\boldsymbol{\Omega}$. However, no significant tendency for the velocity vector to align itself perpendicular to $\boldsymbol{\Omega}$ was noted. Although not central to this study, an important focus of this previous work, along with the simulations of Mansour, Cambon & Speziale (1991*a*, 1992), has been the statistics of the transfer in the limit $R_o \to 0$. In all cases the cascade was shown to be reduced by the rotation, resulting in decreased energy dissipation. At low R_o, the timescale disparity between slow highly nonlinear two-dimensional modes and quasi-linear

inertial waves increases. We can therefore define two distinct timescales: a linear timescale, $\tau_L \sim (2\Omega)^{-1}$, associated with the inertial waves and a nonlinear timescale, $\tau_{NL} \sim U^2/\epsilon$, associated with the turbulent cascade. Here, U is a characteristic velocity scale and we interpret the dissipation rate, ϵ, as the turbulent downscale flux of energy in the infinite Reynolds number (R_e) limit. As $R_o \to 0$, the timescale disparity reduces the nonlinear coupling between turbulence and waves, yielding $\tau_L \to 0$ and $\tau_{NL} \to \infty$.

As a measure of the influence of rotation on τ_{NL} Mansour *et al.* (1991*a*, 1992) have numerically studied the longitudinal velocity derivative skewness (perpendicular to $\boldsymbol{\Omega}$) as a function of R_o. The skewness of a function y is $S(y) = \langle y^3 \rangle / \langle y^2 \rangle^{3/2}$ and $S(-\partial u_1/\partial x_1)$ is a measure of the strength of vortex tube stretching and therefore of the three-dimensional cascade in isotropic turbulence (see e.g. Lesieur 1990). Although their definition of the Rossby number was not identical to that used here, Mansour *et al.* (1991*a*) proposed

$$S\left(-\frac{\partial u_1}{\partial x_1}\right) = \frac{0.49}{[1 + 2/(R_e R_o^2)]^{1/2}}, \tag{1}$$

as a reasonable fit to their simulation data, where the asymptotic value 0.49 is borrowed from the infinite-Reynolds-number isotropic three-dimensional EDQNM calculation of André & Lesieur (1977). They observed that at low R_o the cascade is inhibited by the inertial waves. In this régime it can be shown that at large Reynolds number the nonlinearity collapses onto a set of resonantly interacting triads (e.g. Holloway 1979). Inertial-wave modes can then be expressed as the product of a sinusoidal oscillation (with the linear wave period $2\pi/\sigma(\boldsymbol{k}) \sim O(\tau_L)$) and a slowly-varying amplitude whose time variability scales like $\tau_{NL} \sim R_o^{-1}$. As R_o decreases, the nonlinear term becomes weak relative to the Coriolis term and the inertial-wave amplitudes vary increasingly slowly. However, with the appropriate scaling of time, the flow evolves nonlinearly and the resonant interactions are seen to become increasingly predominant with respect to off-resonant interactions. Whether resonant interactions alone can produce a two-dimensionalization of initially three-dimensional turbulence remains to be seen. However, using his 'instability assumption', Waleffe (1993) reasoned that resonant interactions of inertial waves systematically act to transfer energy towards larger lengthscales in the direction parallel to Ω. In the low-R_o régime, two-dimensionalization, if it occurs at all, does so over a very long timescale, i.e. $\tau_{NL} \to \infty$. For decaying turbulence, two-dimensionalization as $R_o \to 0$ may conceivably never be achieved. However, in geophysical turbulence, where external forcing maintains statistical stationarity, a slow systematic transfer could eventually two-dimensionalize the flow. The simulations of Mansour *et al.* (1991*a*, 1992) also display a significant dependence on the Reynolds number. For this reason, their observation of an extreme inhibition of the three-dimensional cascade at low R_o was demonstrated to be a consequence of the relatively low R_e of their direct numerical simulations. To illustrate this, one can introduce a dissipative timescale, $\tau_D(k) \sim [\nu k^2]^{-1}$, where ν is the viscosity coefficient. In the low-R_o limit $\tau_{NL} \to \infty$ and, if we take the limit $R_e \to 0$, there is the possibility that $\tau_{NL} \gg \tau_D$ for all k. In this case, numerical simulations show only a decay of the quasi-linear inertial waves due to viscosity.

Reynolds (1989) and Mansour, Shih & Reynolds (1991*b*) used rapid distortion theory (RDT) to show that an initially anisotropic Reynolds tensor can be rapidly driven back to isotropy by the rotation. Rather than a Taylor–Proudman two-dimensionalization, they showed that the final state depended on the initial anisotropy. We emphasize that in these studies the focus was on the linear evolution over the

timescale τ_L. In the present study we are concerned with long-lived coherent structures in fully nonlinear flows and therefore concentrate on timescales of the order of many τ_{NL}. In this respect we contend that two-dimensionalization on the slow timescale remains a possibility.

The purpose of this paper is to investigate the formation and stability of quasi-two-dimensional coherent structures, and the possible emergence of vorticity asymmetry, as a function of rotation in the homogeneous case. Clearly, the vorticity asymmetry is of importance in geophysical flows since the effect may limit the ability of rotation to render certain anticyclonic eddies two-dimensional. The centrifugal stability argument shows that maximum anticyclonic destabilization occurs when the eddy vorticity is of the same order as the planetary rotation, implying an application to mesoscale atmospheric vortices with timescales of the order of a day. The numerical results from a series of simulations initialized with the fields from a preliminary two-dimensional decay simulation are presented in §3. The initial fields characterize an advanced state of two-dimensional decay and are dominated by intense isolated vortices. After applying both a weak three-dimensional perturbation and solid-body rotation, the vortices are then allowed to evolve three-dimensionally. Without rotation it is found that both cyclones and anticyclones are unstable with three-dimensionalization occurring first in the small scales. Intense longitudinal vortices are formed with vorticity perpendicular to the axis of the two-dimensional vortices. When rotation is applied there is a preferential destabilization of anticyclones at $R_o \sim O(1)$ and two-dimensional stability is observed at very low R_o. Section 4 presents the results of simulations obtained with isotropic three-dimensional initial conditions, resulting from a non-rotating decay simulation. When rotation is added at $R_o \sim O(1)$ there is a preferential organization of two-dimensional cyclonic structures. At lower R_o, both cyclonic and anticyclonic two-dimensional structures are observed. The conclusions are discussed in §5.

2. The numerical strategy

Triply periodic pseudo-spectral calculations (Orszag 1971) were performed. This has become the standard technique in homogeneous turbulence studies and has been used by Roy (1986), Mansour *et al.* (1991*a*, 1992) and others. We specifically chose a modest resolution (64^3), permitting longer integration times, in order to simulate two-dimensionalization and vorticity asymmetry on the slow timescale τ_{NL}. The model integrated the Navier–Stokes equations in the form

$$\left(\partial/\partial t + \nu k^2 + 2\boldsymbol{\Omega}\times\right)\hat{\boldsymbol{u}}(\boldsymbol{k},t) = \Pi(\boldsymbol{k})\left[F[F^{-1}(\hat{\boldsymbol{u}}(\boldsymbol{k},t)) \times F^{-1}(\hat{\boldsymbol{\omega}}(\boldsymbol{k},t))]\right], \qquad (2)$$

where $\boldsymbol{k}$ is the wavevector, $\hat{\boldsymbol{u}}(\boldsymbol{k},t)$ is the Fourier-space velocity satisfying $\boldsymbol{k}\cdot\hat{\boldsymbol{u}}(\boldsymbol{k},t) = 0$, $\Pi(\boldsymbol{k})$ is the projection operator, F represents a discrete Fourier transform and $\hat{\boldsymbol{\omega}}(\boldsymbol{k},t)$ is the vorticity. The Coriolis term was treated explicitly in the present study and implicitly by Mansour *et al.* (1991*a*, 1992). The disadvantage of the explicit formulation is the small timestep required at low R_o. Since we are primarily concerned with the vorticity asymmetry at $R_o \sim O(1)$, this does not pose too great a problem. However, in §4.2 where low-R_o simulations are discussed, it was necessary to scale the timestep with Ω^{-1} as the Rossby number decreased from unity.

The treatment of the dissipation term is particularly critical in a study of the dynamics of quasi-two-dimensional coherent structures, where timescales characteristic of formation, evolution and pairings are very much longer than the large-scale turnover time, τ_{NL}. In order to simulate such behaviour in direct numerical simulations (DNS),

it is necessary that the dissipative timescale, $\tau_D(k)$ not exceed the nonlinear timescale over a significant spectral range. In three dimensions this is not possible at any resolution accessible to current supercomputers. For example, a comparison between the direct numerical simulations performed at 64^3 resolution by Herring & Métais (1989) with those at 240^3 by Vincent & Meneguzzi (1991) show similar statistical characteristics with neither displaying significant scaling ranges. With rotation, Mansour *et al.* (1991*a*, 1992) detect the dependence on R_e given in (1), which is necessarily quite low for our DNS at 64^3. We therefore decided also to consider two sets of simulations with less dissipation. Large-eddy simulations (LES), in which the viscous term in (2) is replaced by a term based on a spatially and temporally variable turbulent viscosity, $\nu_t(\boldsymbol{x}, t)$ were also performed. In the homogeneous case Chollet & Lesieur (1981) found that ν_t can be approximated by

$$\nu_t(t) = 0.4 \left[\frac{E(k_T, t)}{k_T}\right]^{1/2}.$$

Métais & Lesieur (1992) expressed this in physical space by appealing to the second-order velocity structure function

$$F_2(\boldsymbol{x}, r, t) = \frac{\int\int_{|\boldsymbol{r}'|=r} \|\boldsymbol{u}(\boldsymbol{x}+\boldsymbol{r}', t) - \boldsymbol{u}(\boldsymbol{x}, t)\|^2 \, \mathrm{d}^2 r'}{\int\int_{|\boldsymbol{r}'|=r} \mathrm{d}^2 r'}.$$

Assuming a Kolmogorov spectrum $E(k) = C_K \epsilon^{2/3} k^{-5/3}$, it is possible to express ν_t in terms of F_2 evaluated at the truncation scale, $r = \Delta x = \pi/k_T$,

$$\nu_t(\boldsymbol{x}, t) = 0.04 \ \Delta x \ [F_2(\boldsymbol{x}, \Delta x, t)]^{1/2}.$$

If the contribution to the structure function from the resolved part of the flow is denoted $\overline{F_2}$, then the assumption of a Kolmogorov law for wavenumbers above k_T gives

$$F_2(\boldsymbol{x}, \Delta x, t) = 2.53 \ \overline{F_2}(\boldsymbol{x}, \Delta x, t),$$

and finally

$$\nu_t(\boldsymbol{x}, t) = 0.06 \ \Delta x \ [\overline{F_2}(\boldsymbol{x}, \Delta x, t)]^{1/2}.$$

Although the structure-function model is based on isotropic three-dimensional turbulence, it has been applied to stratified flow by Métais & Lesieur (1992) and we apply it here to anisotropic rotating flow in the hope that at least the small scales are not far from isotropy. For more details regarding the method and a critical assessment of its performance as compared with DNS, the reader is referred to Métais & Lesieur (1992). Also, a particularly simple confinement of the dissipation to near the truncation scale can be effected by replacing the Laplacian operator in the viscous term with an iterated Laplacian. The result is usually referred to as hyperviscosity and has often been used to study the development of coherent structures in two-dimensional flow (e.g. Basdevant & Sadourny 1983). In this study we have employed Δ^8. Since neither subgridscale model accounts directly for the rotation, we compare results using two rather different models as a sensitivity check.

Spherical truncation at wavenumber $k_T = 32$ was applied to the DNS simulations. The LES and hyperviscosity simulations were completely de-aliased by truncation at $2k_T/3$ since, in these cases, the small scales were more energetic. The simulations were initialized with fields characterizing developed two-dimensional or isotropic

three-dimensional turbulence. We define $t = 0$ as the time at which rotation (and the third dimension) was added. All simulations were carried out to a dimensional time of $t = 20$, which is expressed in terms of the integral-scale turnover times in tables 1 and 2. Although the time-series figures cover the dimensional time range $0 \leqslant t \leqslant 20$, we often refer in the text to times as non-dimensionalized by the initial integral-scale turnover time.

In our presentation of the results, we have calculated a number of statistics based on the velocity field in order to compare this study with previous numerical work by Bardina *et al.* (1985), Dang & Roy (1985*a*, *b*), Roy (1986), Teissèdre & Dang (1987) and Mansour *et al.* (1991*a*, 1992). It will be demonstrated that our simulations are consistent with their findings. At the same time, it is our opinion that the interpretation of the results is significantly improved by considering the absolute-vorticity dynamics. For this reason, we also calculate analogous statistical quantities based on the vorticity field. In order to facilitate the description of the results, we refer to the direction parallel to the rotation vector, i.e. $\hat{\boldsymbol{e}}_3$, as the 'vertical'. The kinetic energy and enstrophy

$$E_T = \frac{1}{2}\frac{1}{8\pi^3}\int\int\int \boldsymbol{u}^2(\boldsymbol{r},t)\ \mathrm{d}^3r, \qquad Z_T = \frac{1}{8\pi^3}\int\int\int \boldsymbol{\omega}^2(\boldsymbol{r},t)\ \mathrm{d}^3r,$$

are discussed in terms of two-dimensional and three-dimensional spectral contributions,

$$E_T = E_{2D} + E_{3D}, \qquad Z_T = Z_{2D} + Z_{3D},$$

where

$$Q_{2D} = \sum_{\boldsymbol{k}} q(k_1, k_2, k_3 = 0), \qquad Q_{3D} = \sum_{\boldsymbol{k}} q(k_1, k_2, k_3 \neq 0)$$

and $q(\boldsymbol{k})$ is the corresponding modal quantity. The first term results from the two-dimensional flow, while the second term sums over the vertically varying modes.

3. Simulations with quasi-two-dimensional initial conditions

In this section a series of simulations describing the evolution of initially quasi-two-dimensional eddies in a rotating three-dimensional framework is described. In the case of the DNS and hyperviscosity simulations, these eddies were constructed from preliminary integrations of the two-dimensional equations (also with $u_3 = 0$), where we recall that two-dimensional dynamics (i.e. $\partial/\partial x_3 = 0$) are independent of the rotation. Using the same resolution, Fornberg (1977) demonstrated that the vorticity field in decaying two-dimensional turbulence tends to wrap up into intense coherent vortices. Roy (1986) also performed three-dimensional simulations of quasi-two-dimensional flows, but here we examine closely the vorticity asymmetry at $R_o \sim \mathrm{O}(1)$.

The two-dimensional preliminary hyperviscosity simulation was initialized with Fourier-space phases selected randomly between 0 and 2π and energy narrowly concentrated around wavenumber 7, i.e.

$$E_{2D}(k, t = 0) = A_1 \mathrm{e}^{-(k-7)^2}.$$

The growth of vorticity kurtosis was monotonic and by the end of the run several intense vortices of each sign were apparent. Since the DNS run used a Laplacian dissipation, initial conditions concentrated near $k = 7$ did not produce large vorticity intermittency as the dissipation was of the same order as the nonlinearity at the

	DNS	LES	Δ^8
Energy, E_T	2.81	2.81	0.33
Enstrophy, Z_T	9.10	8.85	7.99
Integral scale, L	1.40	1.41	0.54
Turnover time, $\tau = L/u_{rms}$	0.59	0.59	0.67
Integration time	34τ	34τ	30τ

TABLE 1. Initial statistical quantities for simulations from quasi-two-dimensional initial conditions

energy-containing scale (McWilliams 1984). Here we used instead

$$E_{2D}(k, t = 0) = A_2 \begin{cases} 1, & \text{if } k \leqslant 7; \\ 0, & \text{if } k > 7. \end{cases}$$

In order to produce coherent structures, integration times had to be rather long ($t \approx 30 \times 2\pi/[\omega_{2D}]_{rms}$, where $\boldsymbol{\omega} = \omega_{2D}\hat{\boldsymbol{e}}_3$ is the vorticity). We adjusted the A_i in order to get approximately the same final enstrophies in the fields to be used as our three-dimensional initial conditions. These fields display the familiar signature of two-dimensional turbulence, i.e. intermittent vorticity fields with intense isolated extrema, implying large kurtoses, $K(\omega_{2D}) = \langle\omega_{2D}^4\rangle/\langle\omega_{2D}^2\rangle^2$. Since the two-dimensional equations are symmetric in vorticity, we also note a negligeable disymmetry between cyclonic and anticyclonic structures, or equivalently, a near-zero skewness, $S(\omega_{2D})$. For the initial two-dimensional vorticity field we obtained $K(\omega_{2D}) = 8$ and $S(\omega_{2D}) = -0.1$ for the DNS, and $K(\omega_{2D}) = 7$ and $S(\omega_{2D}) = 0.01$ using hyperviscosity. Since the LES subgridscale model cannot be justifiably applied to long-term two-dimensional dynamics, the results of the preliminary two-dimensional DNS experiment were used to initialize a short two-dimensional LES run of approximately 5 large-scale turnover times in order to let the small scales adjust.

To the basic two-dimensional flow a three-dimensional perturbation was added. Apart from the obvious desirable properties such as: small amplitude, a wide range of lengthscales and isotropy, we found that the exact form mattered little. Here, we present simulations using random phases and

$$E_{3D}(k) = A_3 k\, \mathrm{e}^{-k^2/8^2},$$

with A_3 chosen such that the perturbation energy was 10^{-3} that of the two-dimensional flow. Table 1 displays some statistics describing the initial fields.

3.1. *Without rotation*

Since the three-dimensionalization of these structures in the absence of rotation has not been studied in the homogeneous case, and in order to have a basis for comparison when rotation is added, we begin with the case $\Omega = 0$. Time series of the energy and enstrophy are displayed in figure 1. It is clear that the energy has not completely three-dimensionalized. There is more energy in two-dimensional modes than in the more numerous three-dimensional modes even at the end of the runs, whereas the enstrophy is affected by three-dimensional modes earlier. Note also that Z_{2D} decreases monotonically as in a two-dimensional decay simulation. The rapid growth in enstrophy occurs almost exclusively in ω_1 and ω_2, in the form of longitudinal vortices perpendicular to the initial two-dimensional structures. The tendency to isotropize enstrophy before energy suggests that the three-dimensionalization occurs first in the small scales. This can be seen in the kinetic energy spectra displayed

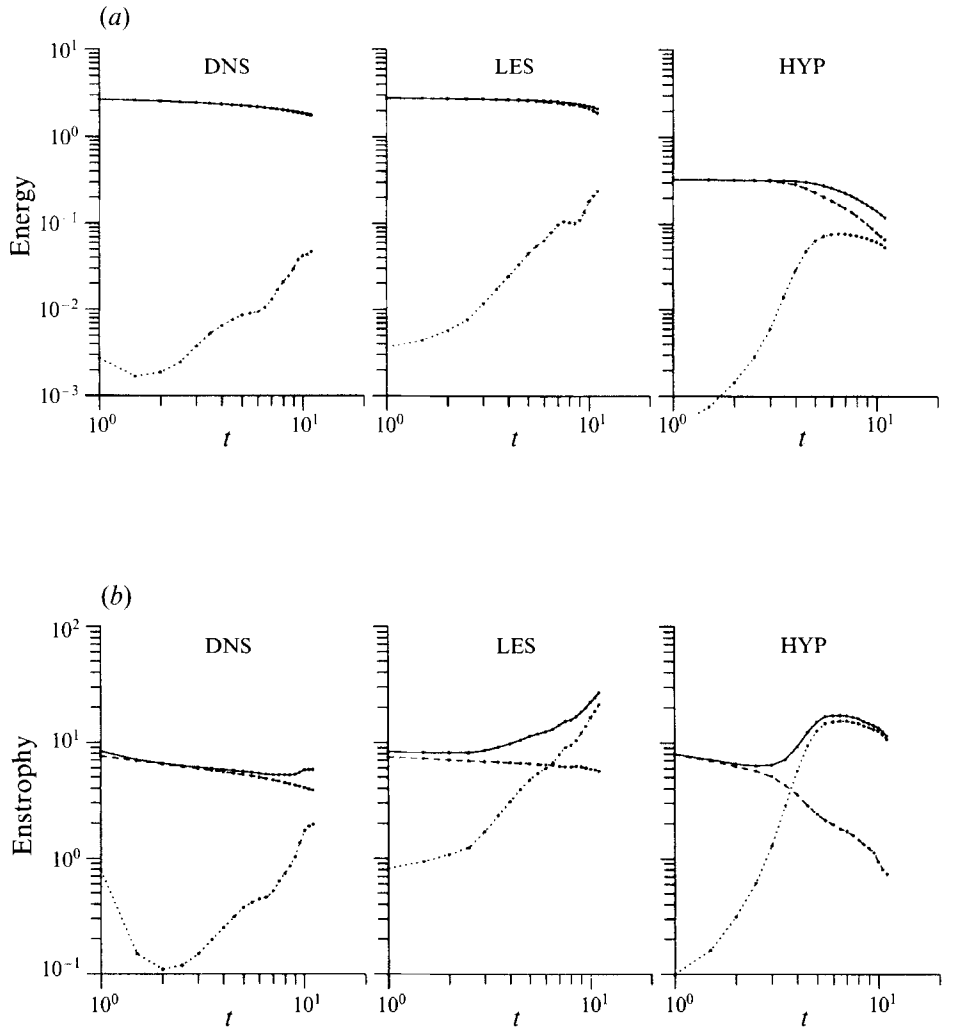

FIGURE 1. Non-rotating simulations with quasi-two-dimensional initial conditions. (*a*) Time series of energy: E_T (solid line), E_{2D} (dashed line) and E_{3D} (dotted line), (*b*) as in (*a*) for the enstrophy Z_T, Z_{2D} and Z_{3D}.

in figure 2 where, by the end of the runs, the flow is approximately isotropic in all but the first few wavenumbers. Although the wavenumber range is small, the final spectrum is visibly less steep at intermediate and large scales than that of the initial conditions.

An examination of the vorticity fields reveals that, by the end of the simulations, the most intense initial vortices are still intact, but less-intense vortices have three-dimensionalized. However, there is a residual two-dimensional component in that intense three-dimensional centres seem to occur in vertical columns identified with the original vortices (see for example figure 6*a* below). This is a manifestation of the coexistence of three-dimensional small scales and two-dimensional large scales. In conjunction with these remnants of the initial field are several intense horizontal structures with vorticity oriented perpendicular to that of the quasi-two-dimensional initial flow. These longitudinal hairpin vortices result from straining by the original

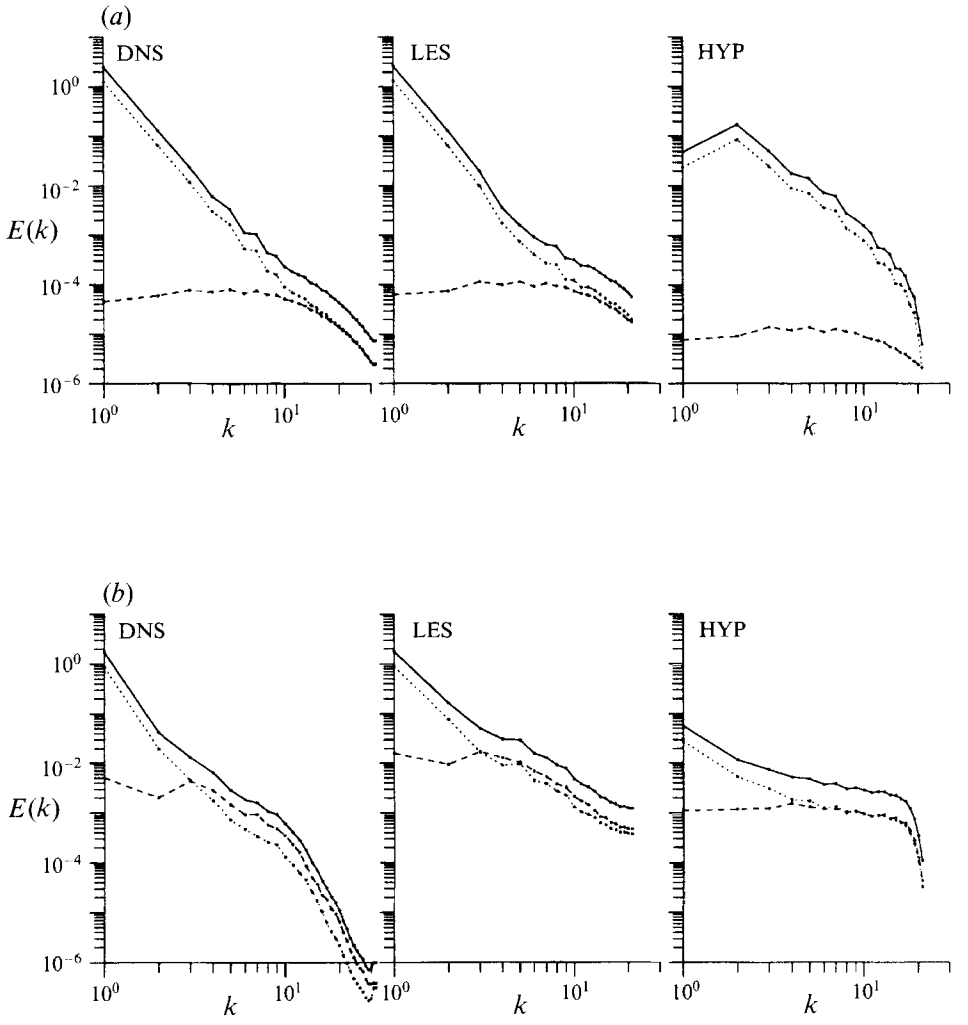

FIGURE 2. Non-rotating simulation with quasi-two-dimensional initial conditions. Energy spectra at (*a*) $t = 0$, (*b*) $t = 20$. $E_T(k)$ (solid line), $\frac{1}{4}\langle u_1^2 + u_2^2\rangle(k)$ (dotted line) and $\frac{1}{2}\langle u_3^2\rangle(k)$ (dashed line).

two-dimensional vortices and have often been observed in three-dimensional studies of shear flows (e.g. Comte, Lesieur & Lamballais 1992).

3.2. *With rotation*

Apart from the value of Ω, these simulations were performed in a manner identical to those described above. We define the Rossby number in terms of the root-mean-square vorticity of the initial quasi-two-dimensional field,

$$R_o = \frac{[\omega_{2D}]_{rms}}{2\Omega}.$$

This definition is perhaps not ideal since stability arguments are more accurately applied to vortex-core vorticities. We have adopted it for convenience as our initial hyperviscosity field is dominated by several vortices of various intensities. However, it

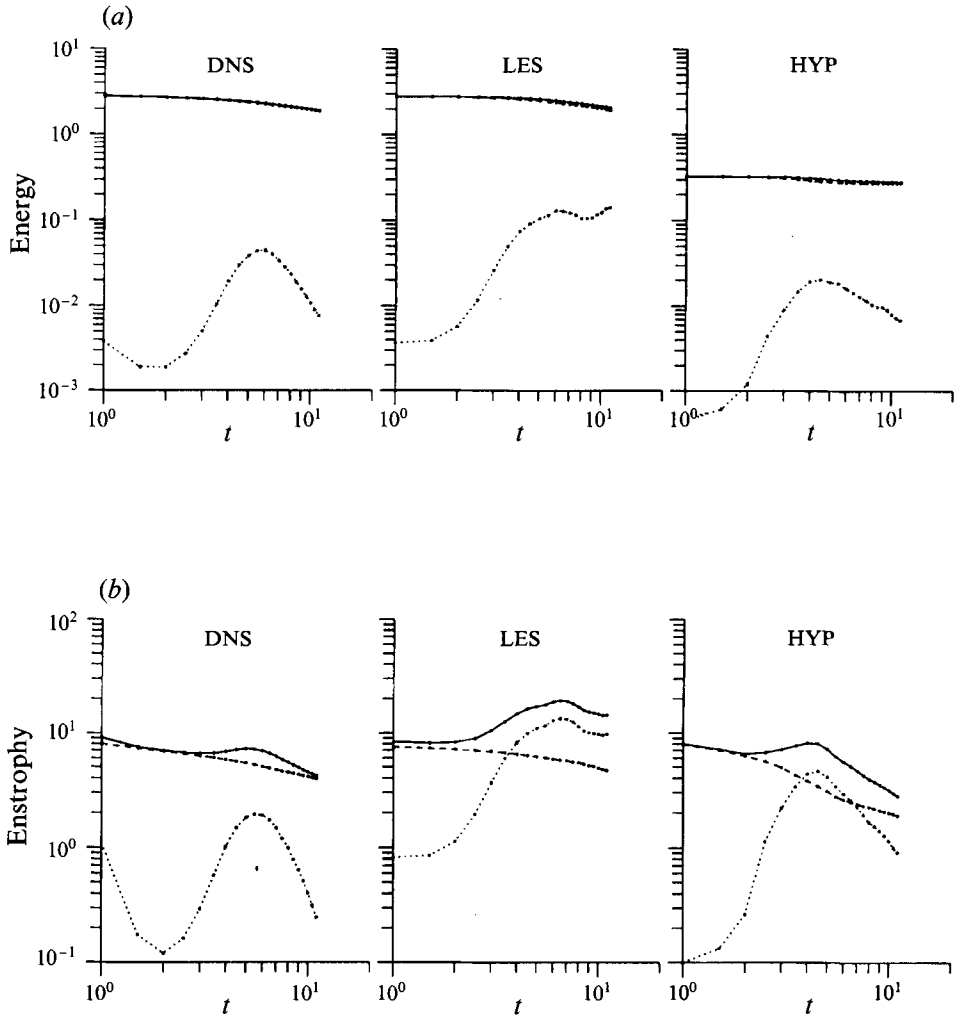

FIGURE 3. As in figure 1 but for the rotating case with $R_o = 1$ and quasi-two-dimensional initial conditions.

should be noted that, in the limit of extreme intermittency, the r.m.s. value will differ greatly from the extremal values.

We describe in detail the simulations with $R_o = 1$ at $t = 0$ and will refer to other simulations as the need arises. Figure 3 shows the energy and enstrophy time-series, where it can be seen that the three-dimensionalization of the large scales, as manifested by E_{3D}, has been inhibited by the rotation, resulting in a reduced energy dissipation particularly evident in the LES and hyperviscosity simulations. The rapid enstrophy growth, corresponding to longitudinal vortex formation, is also less pronounced. However, it occurs earlier at $R_o = 1$ than in the non-rotating case. The final energy spectra (figure 4) are steeper in the small scales than those obtained without rotation (figure 2*b*).

The vorticity fields have been visualized by displaying both a positive and a negative isosurface of ω_3 along with an isosurface of $(\omega_1^2+\omega_2^2)^{1/2}$. In all cases an absolute value

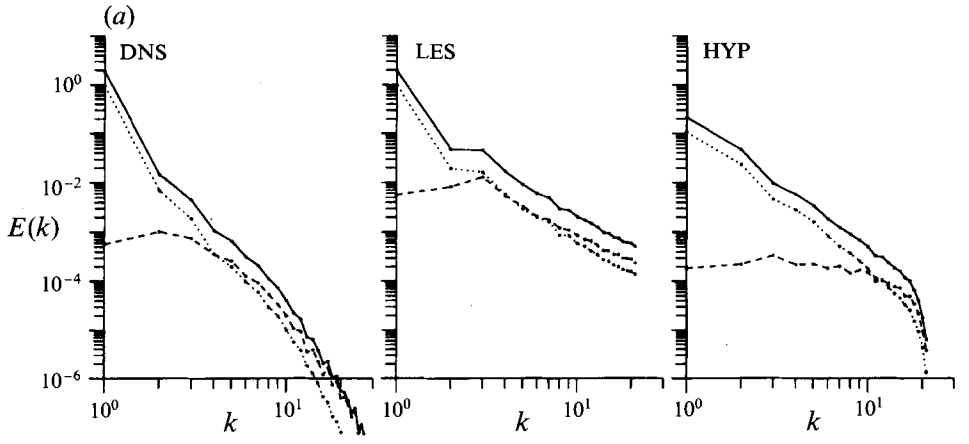

FIGURE 4. As in figure 2 at $t = 20$ but for the rotating case with $R_o = 1$ and quasi-two-dimensional initial conditions.

of twice the root-mean-square vorticity was employed. The initial and final fields are plotted in figure 5, where it can be seen that the original anticyclonic vortices have all been disrupted into three-dimensional structures. In the LES and hyperviscosity simulations a horizontal stretching of these anticyclonic-vorticity structures was also noted. At the same time, the original cyclones show almost no vertical structure.

Simulations were performed with $R_o = 0.1, 0.5, 1, 2$ and ∞ using hyperviscosity. The stability difference between cyclonic and anticyclonic regions diminishes as the Rossby number decreases below unity. In the vorticity fields (figure 6) a quasi-two-dimensional anticyclone is visible at $R_o = 0.5$, although it shows significant vertical structure in the form of a helicoidal perturbation. At $R_o = 0.1$, both E_{3D} and Z_{3D} decreased from their initial values, implying a complete stability of all two-dimensional vortices consistent with the Taylor–Proudman theorem and with simulations performed by Roy (1986). It was only in the low-R_o case, where a return to two-dimensionality was noted, that Roy (1986) examined the vorticity asymmetry. Since the two-dimensional limit is sign-symmetric, he (as we) naturally found no statistical difference between cyclones and anticyclones. The asymmetry can only be noted when R_o is sufficiently large to produce a growing initial three-dimensional perturbation.

4. Simulations with isotropic three-dimensional initial conditions

Calculations were made for decaying homogeneous three-dimensional turbulence submitted to rotation. The isotropic initial fields were generated by non-rotating

FIGURE 5. The vorticity field for the rotating case with $R_o = 1$ and quasi-two-dimensional initial conditions: (*a*) $t = 0$ DNS, (*b*) $t = 20$ DNS; (*c*) $t = 0$ LES, (*d*) $t = 20$ LES; (*e*) $t = 0$ with hyperviscosity, (*f*) $t = 20$ hyperviscosity. The green surface corresponds to $\omega_3 = +\omega_o$, light blue to $\omega_3 = -\omega_o$ and dark blue to $(\omega_1 + \omega_2)^{1/2} = \omega_o$, where $\omega_o = 2\omega_{rms}$.

FIGURE 6. The vorticity field at $t = 20$ for the rotating case with quasi-two-dimensional initial conditions using hyperviscosity at (*a*) $R_o = \infty$, (*b*) $R_o = 2$, (*c*) $R_o = 0.5$ and (*d*) $R_o = 0.1$ (see also figure 5*f* for $R_o = 1$).

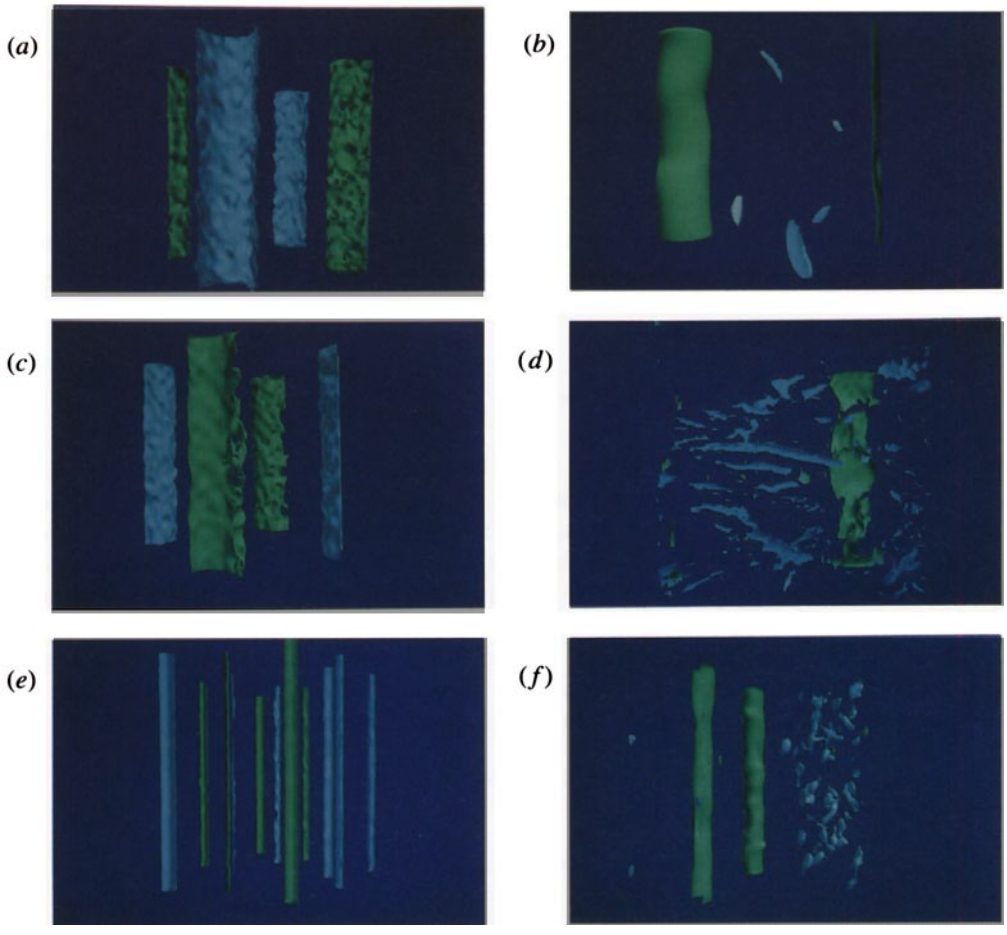

FIGURE 5. For caption see facing page.

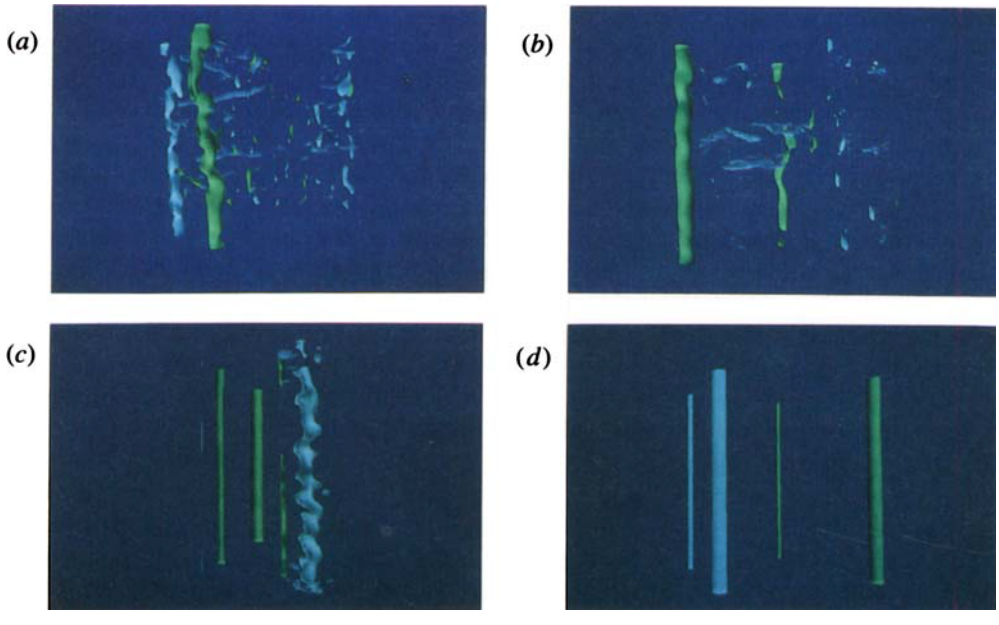

FIGURE 6. For caption see facing page.

	DNS	LES	Δ^8
Energy, E_T	0.33	0.63	1.35
Enstrophy, Z_T	13.4	84.4	137.3
Integral scale, L	0.20	0.18	0.20
Turnover time, $\tau = L/u_{rms}$	0.25	0.16	0.12
Integration time	80τ	130τ	170τ

TABLE 2. Initial statistical quantities for simulations from three-dimensional initial conditions

decay simulations initialized by

$$E(k, t = 0) = A_4 \begin{cases} k, & \text{if } k \leqslant 3; \\ 0, & \text{if } k > 3, \end{cases}$$

with random phases and carried out to near the time of maximum energy dissipation. At this time a short Kolmogorov spectral range was observed in the LES and hyperviscosity simulations. After this, the simulations were continued at various Ω, using otherwise identical parameters with the exception of the DNS viscosity coefficient. In the case of the DNS, the initial spin-up resulted in a significant kinetic energy loss, and a consequent increase in the Kolmogorov scale. For this reason, the viscosity coefficient was reduced from 0.01 to 0.002 at the time rotation was added, yielding a Reynolds number of 81 based on the integral scale and 63 based on the Taylor microscale. Table 2 displays some data characterizing our initial fields.

4.1. *Simulations with* $R_o = 1$

We begin with the simulations with

$$R_o = \frac{[\boldsymbol{\omega} \cdot \boldsymbol{\Omega}]_{rms}}{2\Omega^2} = 1.$$

Examination of the time series of the kinetic energy and its two-dimensional and three-dimensional contributions (figure 7) reveals that for all types of simulations, the two-dimensional energy, E_{2D} decayed significantly less rapidly than the three-dimensional energy, E_{3D}. In fact, E_{2D} increases with time during most of the hyperviscosity simulation, implying a direct transfer from the three-dimensional modes. By the end of all of the runs, the two-dimensional modes account for approximately twice as much energy as the three-dimensional modes. The three-dimensional energy roughly follows a power law, i.e. $E_{3D} \propto t^{-\alpha}$, where $\alpha \approx 1.6$ for the DNS and about 1.0 for the LES and hyperviscosity simulations, in reasonable agreement with high-Reynolds-number isotropic turbulence (see Lesieur 1990 for a discussion). The enstrophy displays a similar behaviour, although the relative weights of two-dimensional to three-dimensional parts of the field are different, owing to the fact that enstrophy weights more heavily the smaller scales and the density of two-dimensional modes increases like $N_{2D} \sim 2\pi k$, whereas $N_{3D} \sim 4\pi k^2$. Still, the decay rate of the two-dimensional enstrophy is weaker than that of its three-dimensional counterpart, implying a monotonic two-dimensionalization of the small scales.

The energy spectra (figure 8) display a progressive steepening throughout the simulations and a developing anisotropy between $u_{1,2}$ and u_3 variance spectra. This first occurs, somewhat surprisingly, in the small scales where the u_3 spectrum exceeds that of the horizontal flow. This anisotropy was noted in the EDQNM study of Cambon & Jacquin (1989) as well as the direct simulations of Teissèdre & Dang

(1987). At the large scales the u_3 variance is in the range of 4 to 7 times weaker than that due to the average horizontal component.

As a measure of component anisotropy, we follow Reynolds (1989) and Mansour *et al.* (1991*b*) and adopt

$$b_{ij}^{a} = \frac{\overline{a_i a_j}}{a^2} - \frac{\delta_{ij}}{3}, \tag{3}$$

where vector $\boldsymbol{a}$ represents velocity or vorticity and $\overline{(-)}$ denotes a spatial average. Time series of the diagonal elements of b_{ij}^{u} and b_{ij}^{ω} are shown in figure 9, where it can be seen that the u_3 variance is decreasing near the end of the simulations and that the vorticity is monotonically evolving to a state dominated by ω_3. The results are consistent with a tendency towards a two-component two-dimensional flow using the terminology of Reynolds (1991). Note also that for approximately the first quarter of the runs the velocity-component anisotropy is weak (especially for DNS). It develops only after approximately 20 initial large-scale turnover times. This is consistent with the rapid distortion theory results of Reynolds (1989) and Mansour *et al.* (1991*b*) who noted no systematic trend to Reynolds-stress anisotropy over the fast timescale, τ_L in the low R_o limit. As pointed out by a reviewer, rapid oscillations in the Reynolds stresses at frequency 4Ω were predicted by Mansour *et al.* (1991*b*). These can perhaps be seen in the time series of b_{ij}^{u} (see also Lesieur *et al.* 1991), although we have made no attempt to sample often enough to measure their frequencies.

Previous researchers have considered the integral scales as a measure of two-dimensionalization in initially-isotropic flows involving rotation (Bardina *et al.* 1985; Dang & Roy 1985*a*, *b*; Roy 1986; Teissèdre & Dang 1987 in simulations, Jacquin *et al.* 1990 in the laboratory). We generalize the concept slightly by introducing a vorticity analogue, i.e.

$$L_{ij,k}^{a} = \frac{1}{a^2} \int_0^\infty \overline{a_i(\boldsymbol{r}) a_j(\boldsymbol{r} + s\hat{\boldsymbol{e}}_k)}\ \mathrm{d}s, \tag{4}$$

where $\boldsymbol{a}$ represents velocity or vorticity. In practice a discretized version is required. We calculated covariances at intervals of one grid length and employed Simpson's rule to perform the integral. It should be kept in mind that the discrete scale $L_{ij,k}^{a}$ is numerically bounded by our periodic domain length such that $L \leqslant \pi/3$ for a three-dimensional isotropic vector. Figure 10 displays $L_{ii,1}^{u}$ and $L_{ii,3}^{u}$. The results are consistent with the above-mentioned studies, although the present simulations are much longer. $L_{11,1}^{u}$ is seen to grow steadily and quasi-linearly as the large scales two-dimensionalize and the spectrum steepens. More striking however, is the large growth in $L_{11,3}^{u}$ which attains values between 5 and 10 times greater than $L_{33,3}^{u}$ by the end of the runs. It must be kept in mind that previous simulations were not integrated significantly longer than the time at which $L_{11,3}^{u} \approx L_{33,3}^{u}$. This is perhaps the most natural way of comparing the length of rotating simulations. Here, $L_{11,3}^{u} \approx L_{33,3}^{u}$ occurred in the first quarter of the runs. Up until this time the velocity component anisotropy did not show a clear trend (figure 9). It would appear that the integral-scale anisotropy growth occurs almost immediately upon application of the rotation, whereas the Reynolds stresses show a trend to anisotropy only after tens of turnover times. In short, Bardina *et al.* (1985), Dang & Roy (1985*a*, *b*), Roy (1986) and Teissèdre & Dang (1987) were able to observe anisotropic $L_{ij,k}^{u}$ in their simulations, but they did not integrate long enough to observe anisotropic Reynolds stresses.

The vorticity-based lengthscales, $L_{ii,1}^{\omega}$ and $L_{ii,3}^{\omega}$ are displayed in figure 11. Here we note the important growth in ω_3 lengthscales in the directions both parallel and

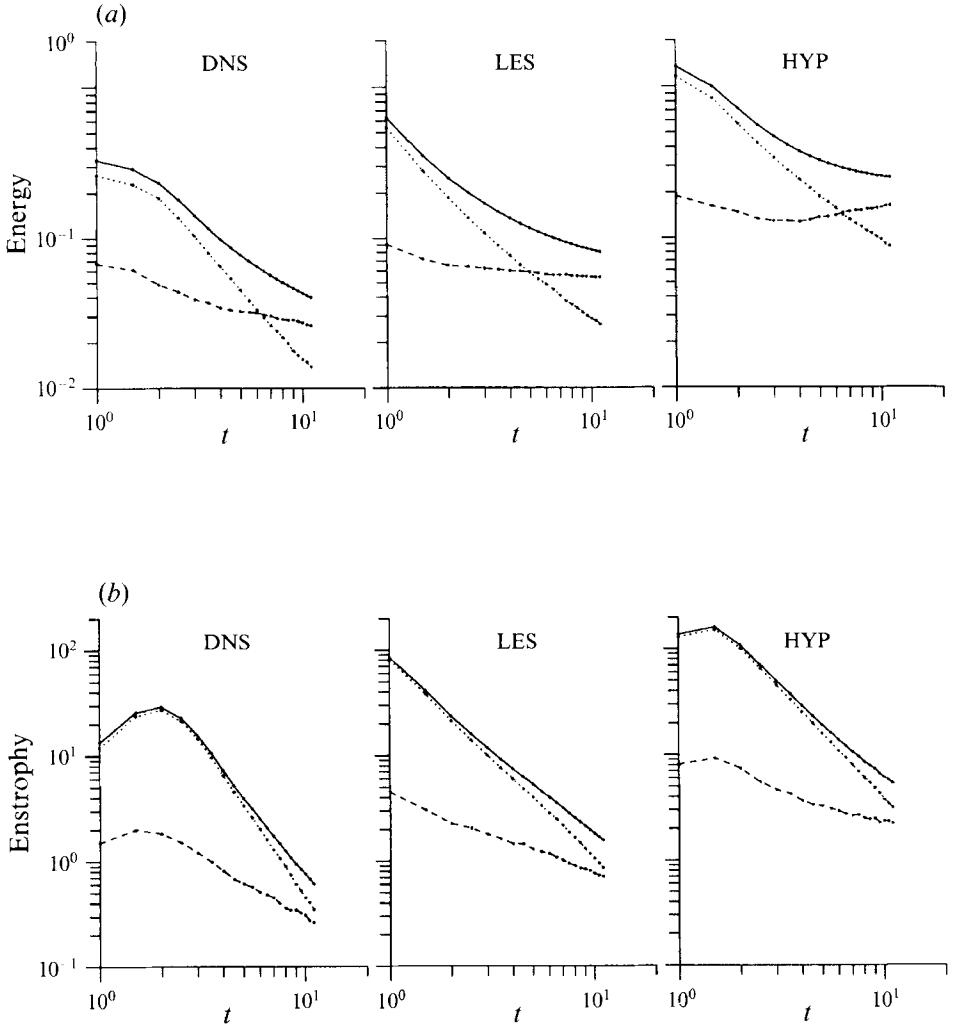

FIGURE 7. As in figure 1 but for the rotating case with $R_o = 1$ and three-dimensional initial conditions.

perpendicular to the axis of rotation. Once again, this is consistent with a two-dimensionalization of the small scales and a consequent steepening of the enstrophy spectrum associated with the formation of two-dimensional coherent structures, larger in horizontal scale than the tube-like high-vorticity regions noted in three dimensions by Siggia (1981) and Vincent & Meneguzzi (1991). In order to distinguish between cyclonic and anticyclonic regions, we have performed the $L^{\omega}_{33,3}$ sum obtained from discretizing (4) separately according to whether $\omega_3(\boldsymbol{r})$ is positive or negative. The resulting curves (figure 11*c*) show correlations over significantly larger vertical scales for cyclonic regions than for anticyclonic regions. Stated simply, cyclonic regions are more two-dimensional.

Both the initial and final vorticity fields are shown in figure 12. Although the results are not convincing for the DNS, the LES and hyperviscosity simulations both display two-dimensional coherent cyclones and little or no two-dimensionalization of the anticyclonic regions. If we reduce the Rossby number from unity to 0.1, the field

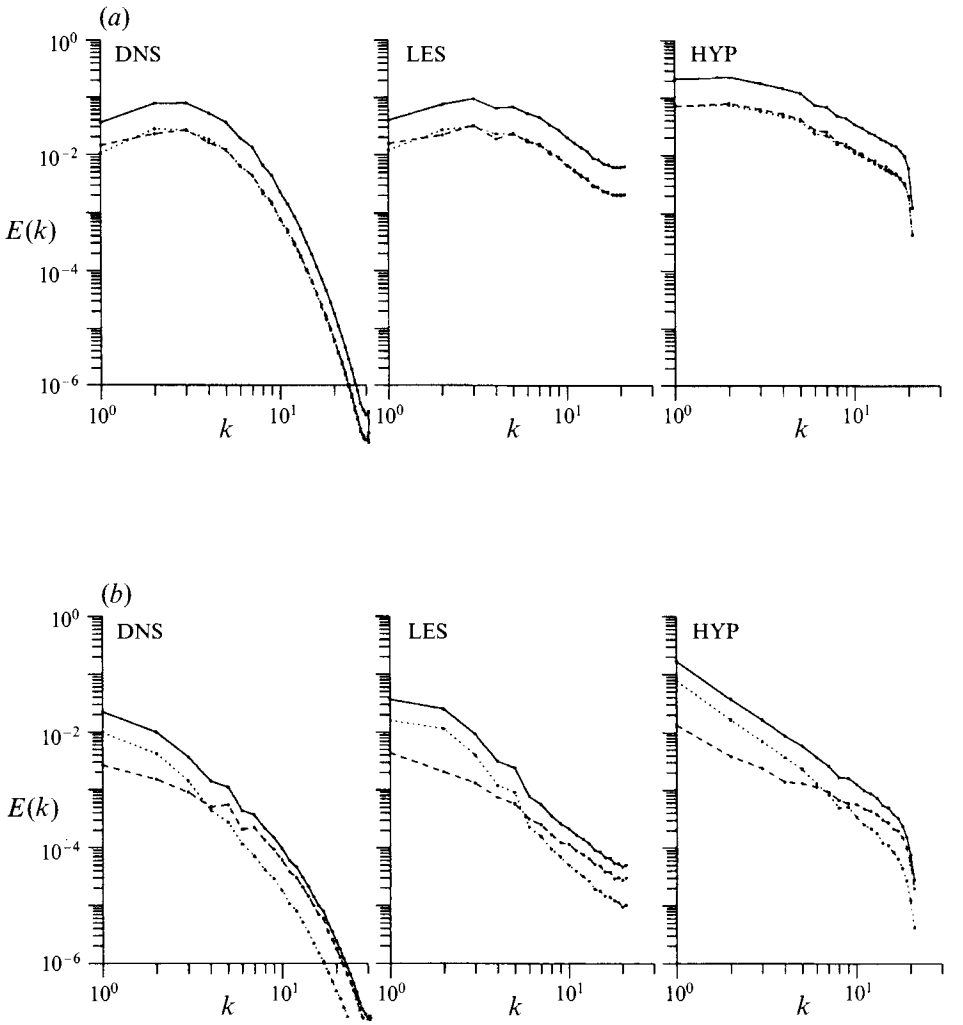

FIGURE 8. As in figure 2 but for the rotating case with $R_o = 1$ and three-dimensional initial conditions.

shown in figure 13 is the result using hyperviscosity. Here it is noted that, at lower R_o, both two-dimensional cyclones and two-dimensional anticyclones emerge from the isotropic initial conditions.

It is well known, as already recalled, that non-rotating isotropic turbulence contains coherent structures in the form of intense vortex tubes, corresponding to low-pressure regions (see also Métais & Lesieur 1992). Consider the initial isotropic flow to which rotation will be applied. Very naively, we can approximate it by a distribution of vortices, each one in the Rossby-number range of maximum anticyclonic instability, which are aligned either parallel or perpendicular to the rotation axis, $\hat{\boldsymbol{e}}_3$. Now we apply the Rayleigh argument to the parallel vortices, yielding a stabilization of the cyclones and a destabilization of the anticyclones. If we use the quasi-two-dimensional initial-condition results of §3 as a guide, the anticyclonic vorticity is stretched longitudinally by the cyclones, which gradually dominate the field. As for the original longitudinal vortices (with $\boldsymbol{\omega} \perp \hat{\boldsymbol{e}}_3$), they are also stretched in the shear

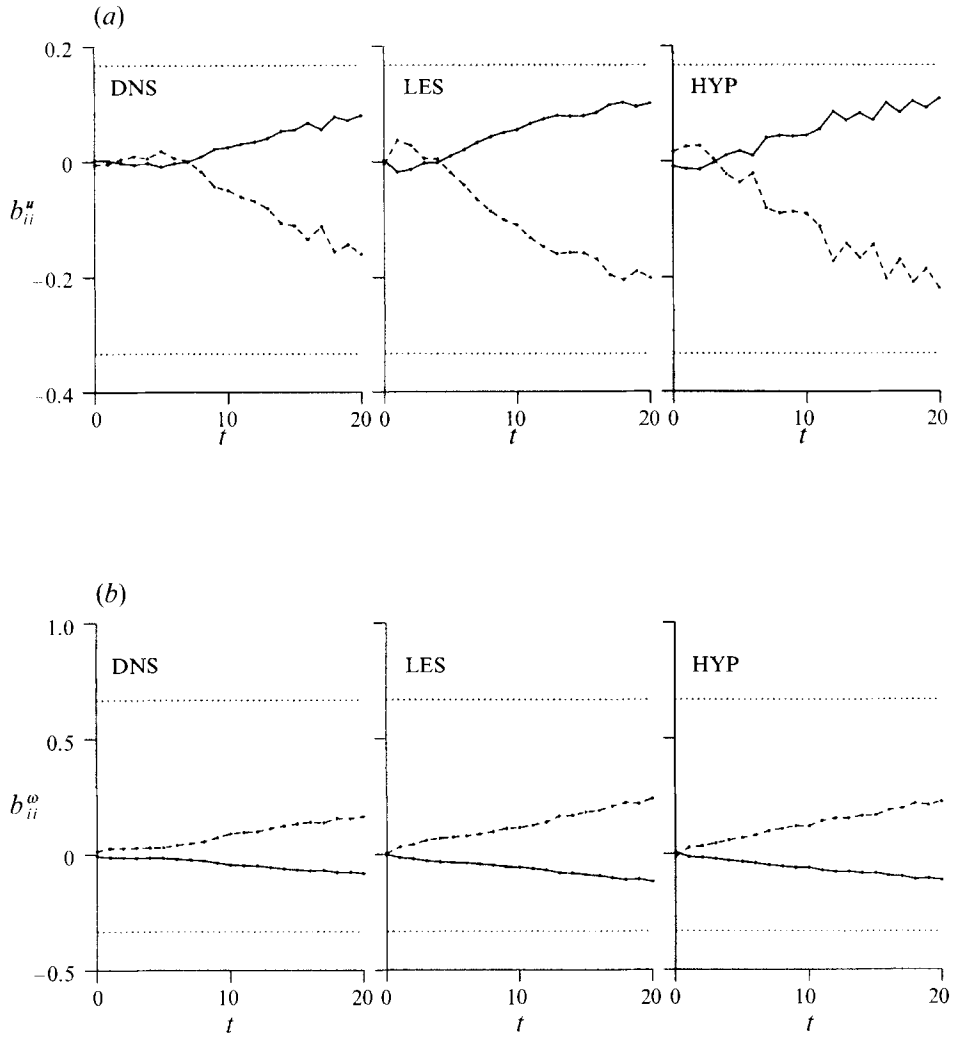

FIGURE 9. $R_o = 1$. Time series of the diagonal elements of the anisotropy tensor (defined in (3)) for (*a*) the velocity and (*b*) the vorticity: component perpendicular to the rotation axis (solid line), component parallel to the rotation axis (dashed line). The dotted lines give values for two-dimensional two-component flow.

induced by the cyclonic vortices. As in the quasi-two-dimensional case, rotation is responsible for a breaking of symmetry in the form of the emergence of cyclonic vortices from the randomly oriented initial vortex distribution. In the subsequent evolution the stretched longitudinal vortices participate in the three-dimensional cascade to the dissipation, whereas the remaining quasi-two-dimensional cyclones evolve in a manner consistent with two-dimensional turbulence studies. Since all intense coherent structures are of the same sign, pairing events are not uncommon, producing an intense inverse energy cascade and eventually an intermittent vorticity field dominated by a few strong vortices.

The instantaneous histogram of grid-point values is often considered as an estimate of the probability density function (p.d.f.), without the required ensemble average. The histograms of ω_3 for the simulations with $R_o = 1$ for the initial and final fields

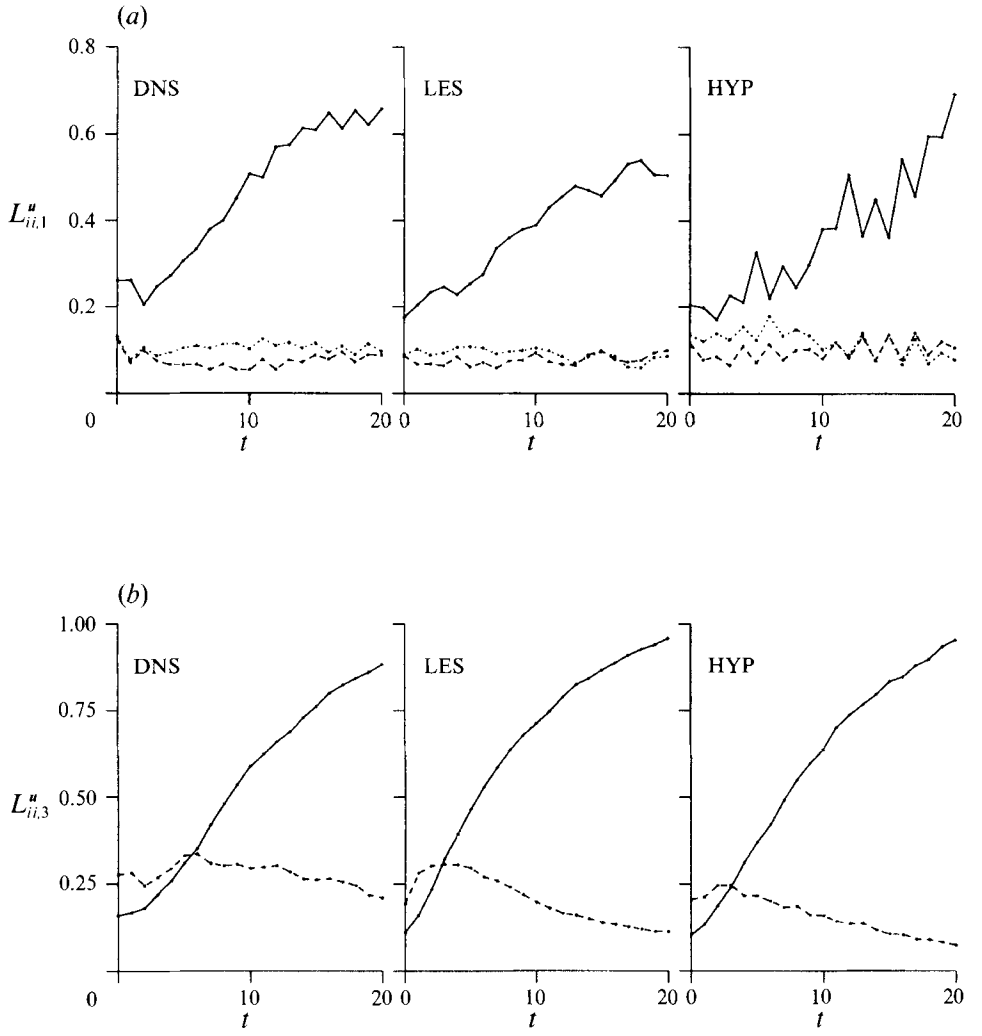

FIGURE 10. $R_\omega = 1$. Time series of the integral scale (*a*) perpendicular to the rotation axis u_1 (solid line), u_2 (dashed line) and u_3 (dotted line); and (*b*) parallel to the rotation axis u_1 (solid line) and u_3 (dashed line).

are shown in figure 14. The initial p.d.f.'s characterize non-rotating three-dimensional turbulence and resemble those obtained from $\partial u_i/\partial x_j$ $(i \neq j)$ both in experiments on grid turbulence and in numerical simulations. We recall that this quantity is not skewed in homogeneous isotropic three-dimensional turbulence. The exponential form noted in simulations by Herring & Métais (1989) and Vincent & Meneguzzi (1991) and in the laboratory by Van Atta & Park (1972) and Anselmet *et al.* (1984) is present. It was proposed by Métais & Lesieur (1992) that this could be the signature of the coherent vortices of isotropic turbulence. The various treatments of the dissipation also give rise to differences in the p.d.f.'s. The fact that the LES p.d.f. shows slightly less intermittency than that of the DNS was noted and discussed in Métais & Lesieur (1992). In comparison, the hyperviscosity simulation shows considerable intermittency and the distinctive exponential form noted at higher R_e by Vincent &

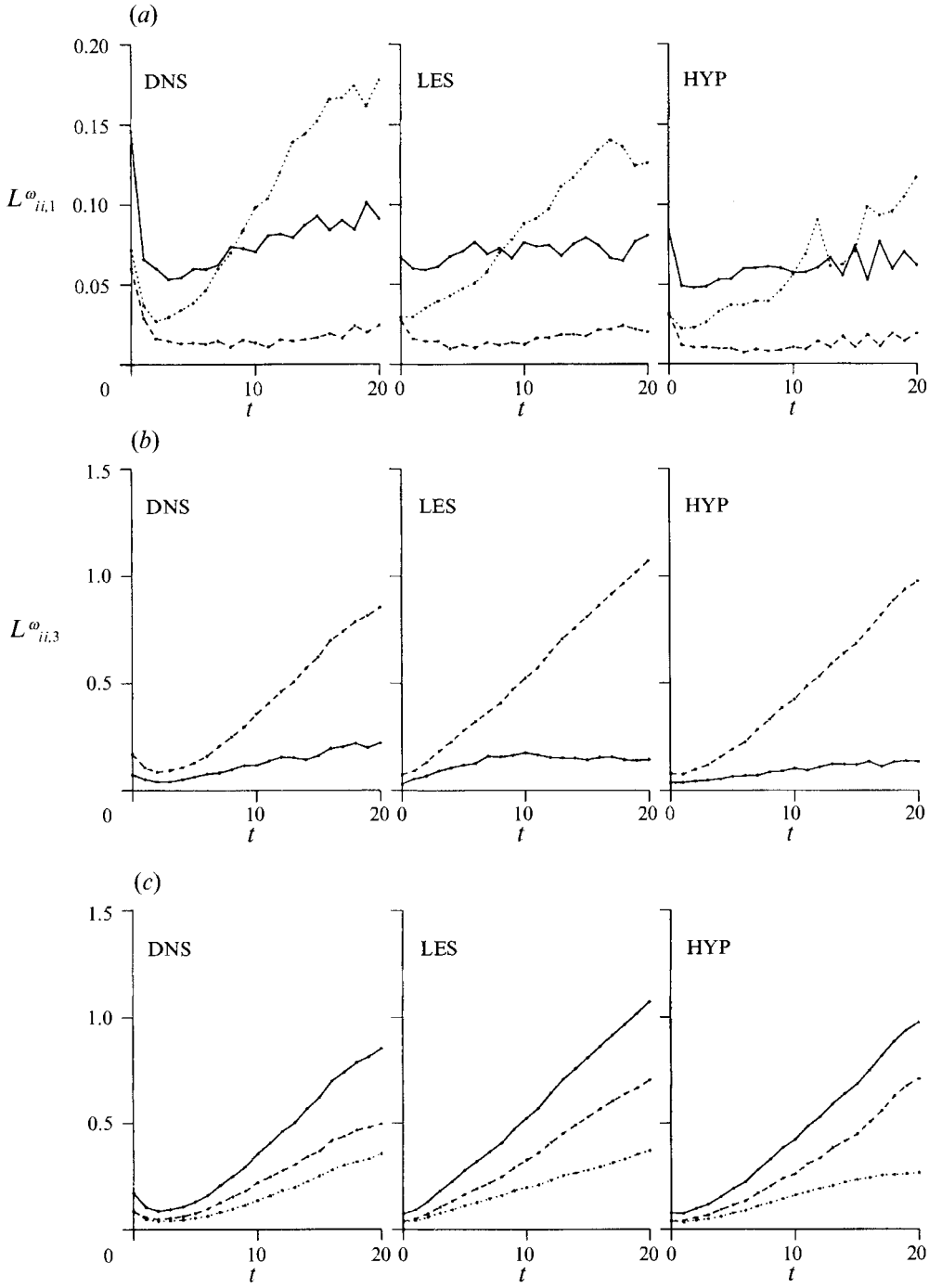

FIGURE 11. $R_o = 1$. Time series of the vorticity-based scale (*a*) perpendicular to the rotation axis ω_1 (solid line), ω_2 (dashed line) and ω_3 (dotted line); (*b*) parallel to the rotation axis ω_1 (solid line) and ω_3 (dashed line); and (*c*) decomposition of $L^{\omega}_{33,3}$ (solid line) into cyclonic (dashed) and anticyclonic (dotted) contributions.

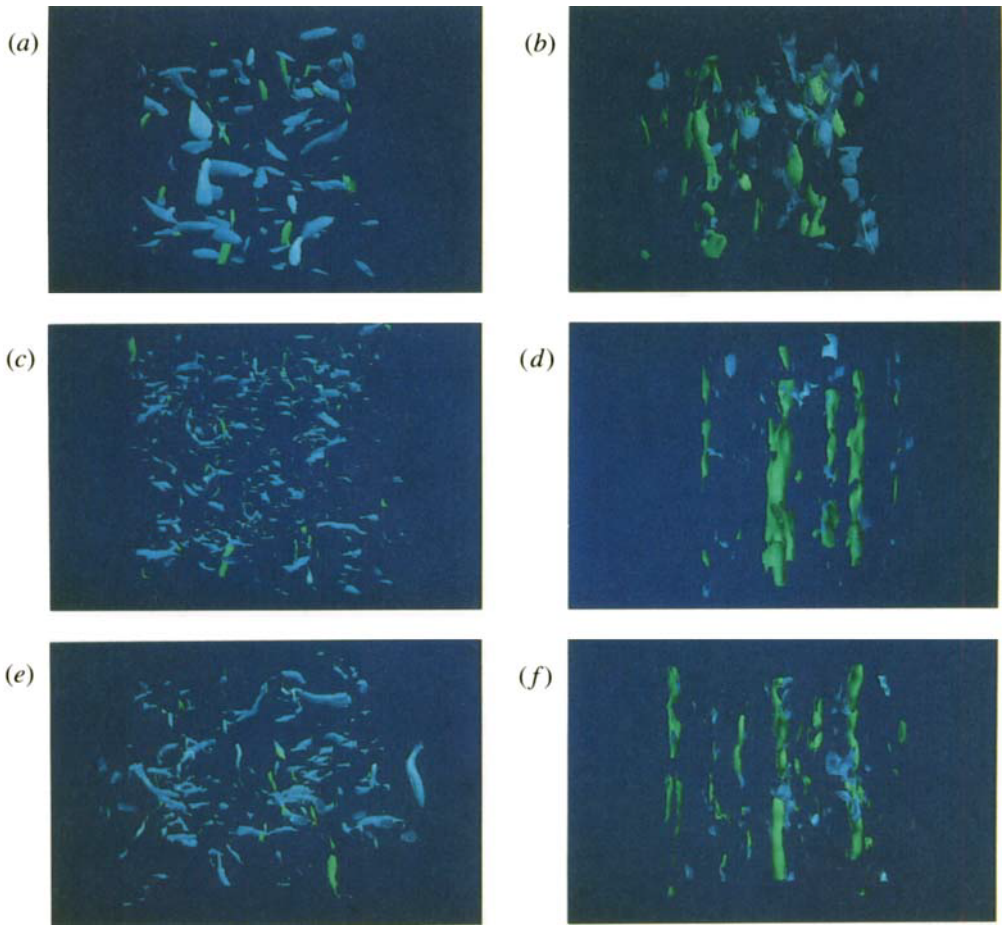

FIGURE 12. The vorticity field for the rotating case with $R_o = 1$ and three-dimensional initial conditions as in figure 5: (*a*) $t = 0$ DNS, (*b*) $t = 20$ DNS; (*c*) $t = 0$ LES, (*d*) $t = 20$ LES; (*e*) $t = 0$ with hyperviscosity, (*f*) $t = 20$ hyperviscosity.

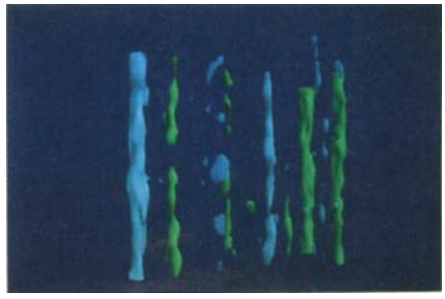

FIGURE 13. The vorticity field at $t = 20$ for the rotating case with $R_o = 0.1$ and three-dimensional initial conditions using hyperviscosity.

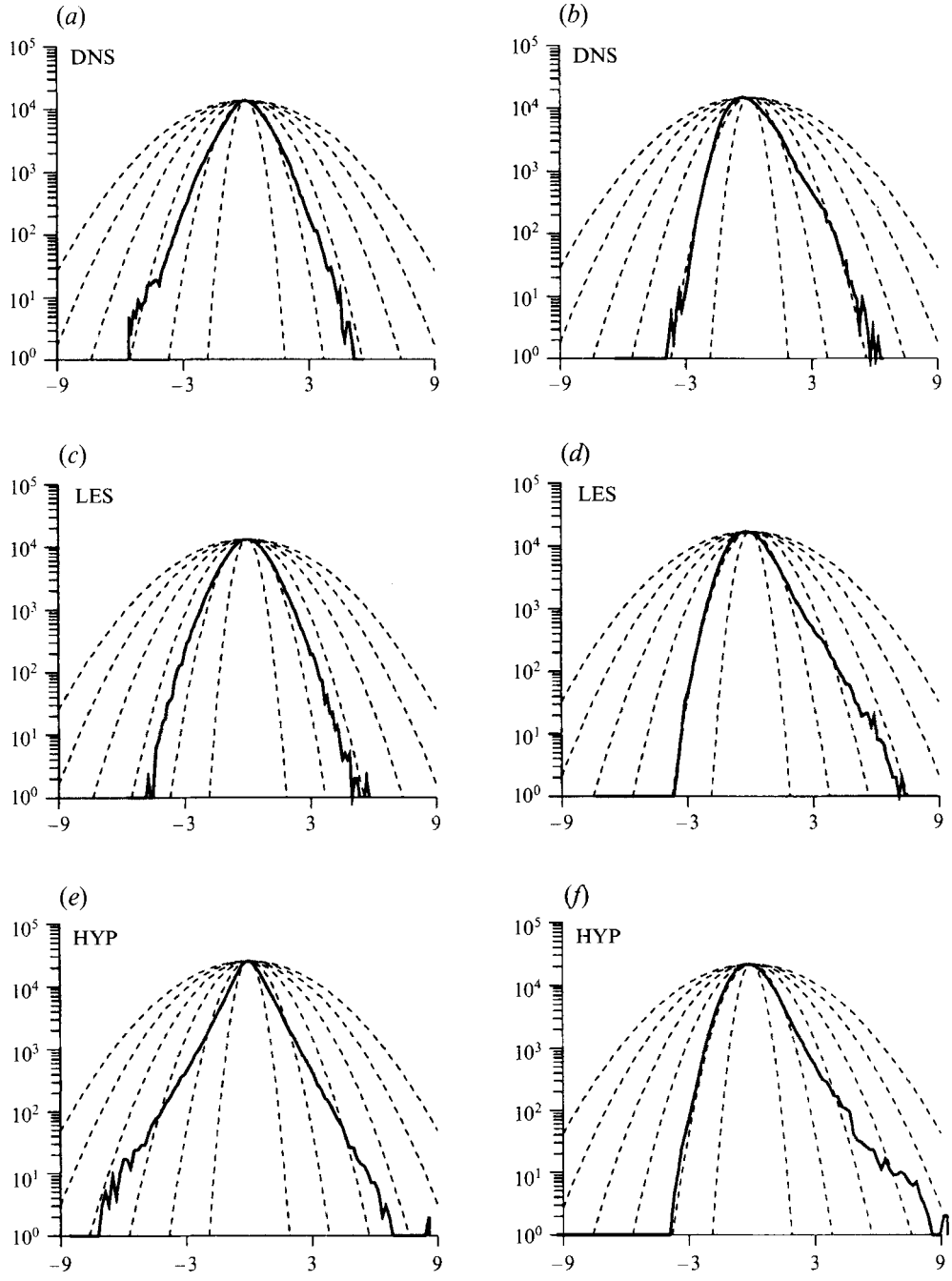

FIGURE 14. $R_o = 1$. Grid-point value histograms of ω_3: (*a*) $t = 0$ DNS, (*b*) $t = 20$ DNS; (*c*) $t = 0$ LES, (*d*) $t = 20$ LES; (*e*) $t = 0$ with hyperviscosity and (*f*) $t = 20$ hyperviscosity. The dashed lines correspond to comparison Gaussian functions of various widths. The fields have been scaled by their r.m.s. values.

Meneguzzi (1991). These differences underline the importance of comparing results using different subgridscale models.

The p.d.f.'s at the end of the runs differ considerably from their non-rotating counterparts at $t = 0$ for all treatments of the dissipation. The $t = 20\ \omega_3$ histogram shows a perceptible asymmetry. The decay on the positive (cyclonic) side is not only slower than Gaussian, but also slower than in the non-rotating initial fields, implying considerable cyclonic intermittency. We have seen above that this occurs in the form of quasi-two-dimensional coherent structures. On the other hand, the negative side of the distribution (anticyclonic) displays an almost perfectly Gaussian behaviour. Anticyclonic regions therefore show no intermittency. In other words, the anticyclonic vortices existing in the initial fields have been destroyed by the rotation, while the cyclonic vortices have been reinforced. The Gaussian behaviour also suggests that the three-dimensional anticyclonic regions are not participating in the cascade of energy to small scales. The p.d.f.'s of the vorticity components perpendicular to the rotation axis (not shown) are little affected by the rotation and therefore resemble those displayed in figure 14 at $t = 0$.

The asymmetry in the ω_3 field can be measured by its skewness. Time series of $S(\omega_i)$ are shown in figure 15, where the growth in $S(\omega_3)$ is apparent while $S(\omega_{1,2})$ oscillate about zero. On the same figure the kurtosis time series are also displayed. McWilliams (1984) used this quantity to signal the emergence of two-dimensional coherent structures. Although these structures are apparent in the LES and hyperviscosity simulations, the low R_e of the DNS prevents the buildup of significant vorticity intermittency. This has long been known for two-dimensional flows (McWilliams 1984) and explains the frequent use of hyperviscosity in two-dimensional simulations.

4.2. *The dependence on R_o*

Having described the effect of rotation at $R_o = 1$, we now consider other rotation rates. For this purpose we have performed 14 simulations of 25 integral-scale turnover times duration employing hyperviscosity and starting from the same initial conditions as above. The only parameter varied is the rotation rate, which produces almost 4 orders of magnitude variation in the Rossby number. The normalized energy dissipation along with its two-dimensional and three-dimensional contributions can be written

$$\mathscr{D}_T = -\frac{1}{E_o}\frac{\Delta E_T}{\Delta t}, \qquad \mathscr{D}_{2D} = -\frac{1}{E_o}\frac{\Delta E_{2D}}{\Delta t}, \qquad \mathscr{D}_{3D} = -\frac{1}{E_o}\frac{\Delta E_{3D}}{\Delta t}, \tag{5}$$

where $E_o = E_T(t = 0)$, Δ refers to differences over the 25τ integration length and τ is the integral-scale turnover time. They are plotted in figure 16(*a*). Starting from low rotation rates, large R_o, the curves are somewhat flat as the rotation is too slow to affect the flow significantly. Near $R_o = 1$ the total dissipation begins to drop off as the inertial waves inhibit the cascade (Cambon & Jacquin 1989; Mansour *et al.* 1991*a*, 1992), reaching very low values at the lowest R_o. Over the range $0.05 < R_o < 0.7$ the dissipation of the two-dimensional modes changes sign as these modes actually gain energy via a transfer from three-dimensional modes. This direct conversion from three-dimensional to two-dimensional energy reaches a maximum at $R_o = 0.2$.

The Taylor microscale, $\lambda = (E_T/Z_T)^{1/2}$ is displayed as a function of the Rossby number in figure 16(*b*). This quantity decreases in decaying three-dimensional turbulence and increases in decaying two-dimensional turbulence, reflecting the inverse energy cascade (see McWilliams 1984 who considered $\bar{k} = \lambda^{-1}$). Here we note

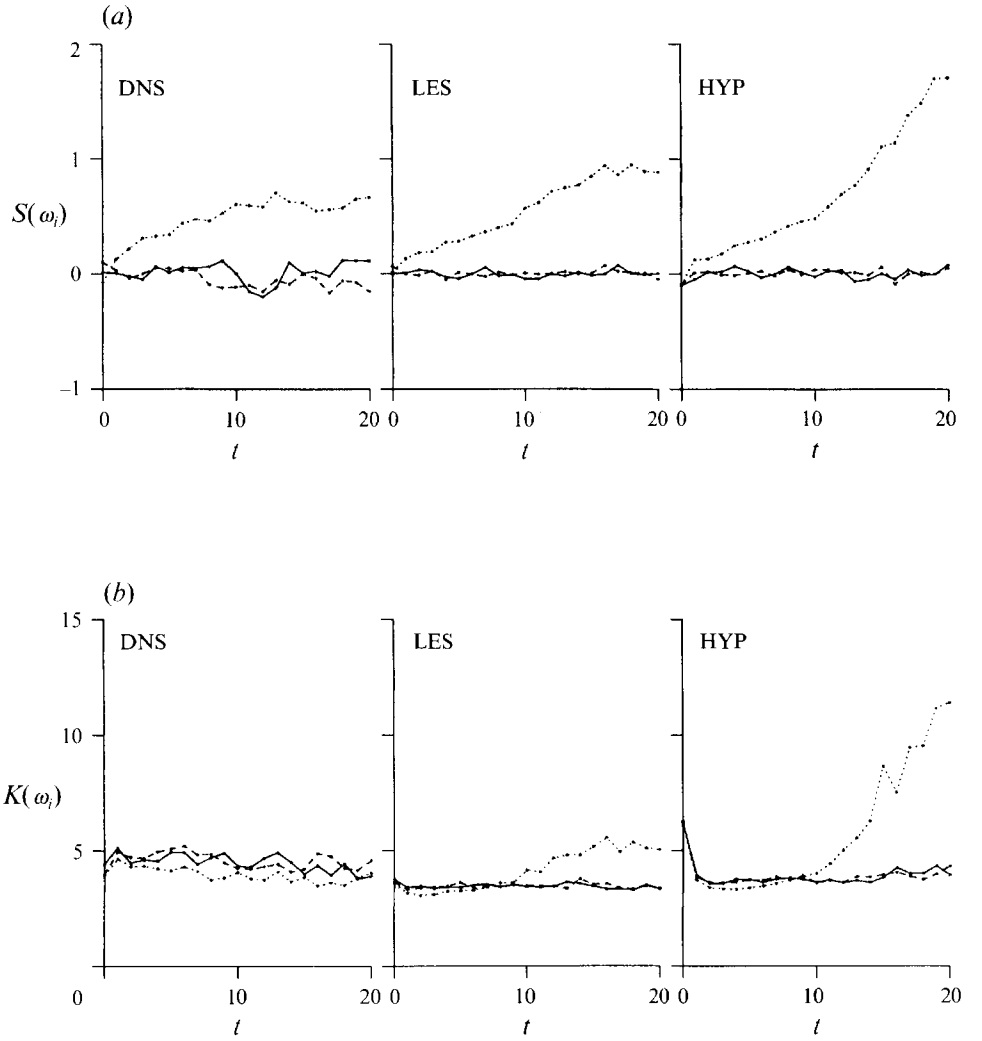

FIGURE 15. $R_o = 1$. Time series of (*a*) vorticity skewness and (*b*) vorticity kurtosis: ω_1 (solid line), ω_2 (dashed line) ω_3 (dotted line).

three-dimensional behaviour at large R_o and two-dimensional behaviour at small R_o. More importantly, a maximum is reached near $R_o = 0.1$ where the inverse cascade is strongest.

The two-dimensionalization of the velocity and vorticity over the time period simulated is shown in figure 16c. It is measured by the spectral anisotropy growth,

$$\mathscr{A}_E = \frac{E_{2D}(t = 25\tau)/E_{3D}(t = 25\tau)}{E_{2D}(t = 0)/E_{3D}(t = 0)}, \qquad \mathscr{A}_Z = \frac{Z_{2D}(t = 25\tau)/Z_{3D}(t = 25\tau)}{Z_{2D}(t = 0)/Z_{3D}(t = 0)}. \tag{6}$$

It can be seen that the two-dimensionalization of the velocity field reaches a maximum near that of the three-dimensional–two-dimensional transfer (seen in figure 16*a*). One can observe the same behaviour in the study of Roy (1986) who plotted time series of the vertical integral scales $L^u_{11,3}$ and $L^u_{33,3}$ at various R_o in his figure 97. A clear maximum $L^u_{11,3}$ growth at his integral-scale based Rossby number of 0.35 can be

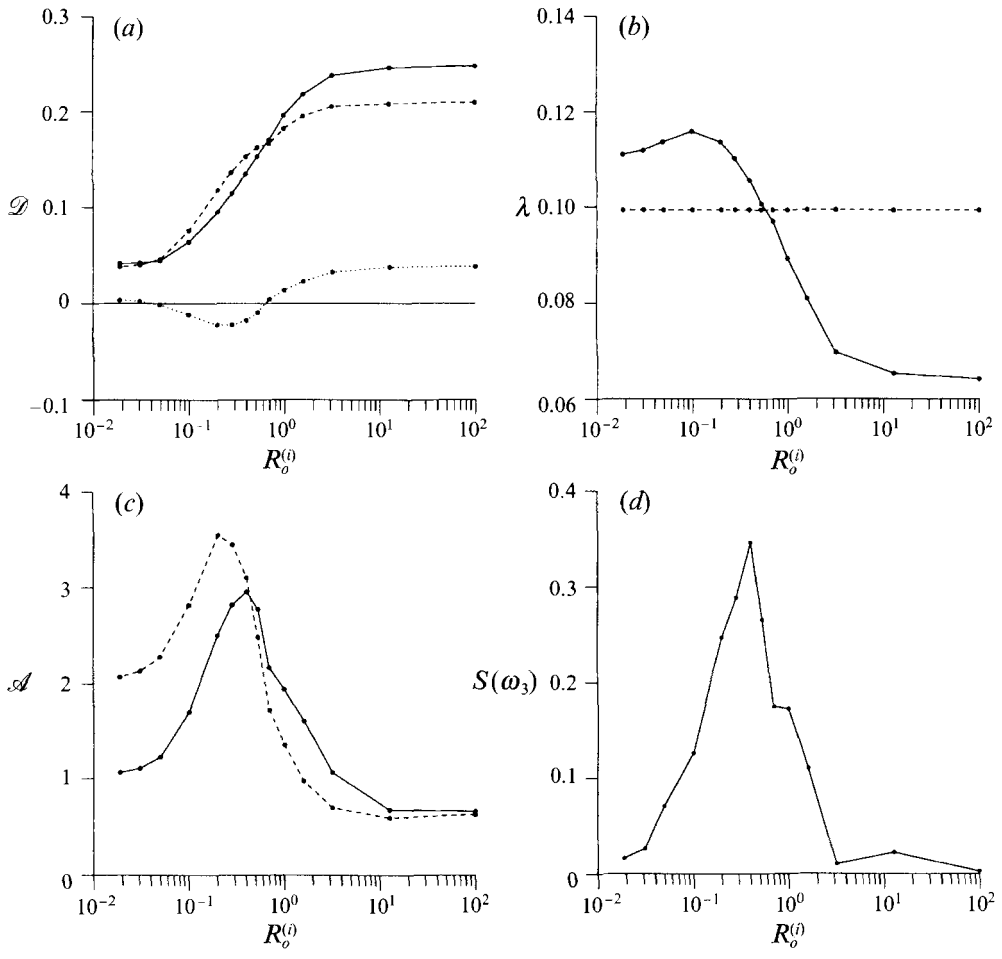

FIGURE 16. The result of varying the initial Rossby number, $R_o^{(i)}$ in simulations of 25 turnover times duration from three-dimensional initial conditions using hyperviscosity. (*a*) Normalized energy dissipation: $\mathscr{D}_T$ (solid line), $\mathscr{D}_{2D}$ (dotted line), $\mathscr{D}_{3D}$ (dashed line) (see (5) in text); (*b*) Taylor microscale at the beginning (dashed) and at the end (solid) of the simulation; (*c*) spectral anisotropy growth: $\mathscr{A}_E$ (solid line) and $\mathscr{A}_Z$ (dashed line) (see (6) in text); (*d*) vorticity skewness, $S(\omega_3)$.

seen. The two-dimensionalization, as measured here, then decreases to near unity at low R_o, consistent with Mansour *et al.* (1991, 1992). The vorticity is seen to two-dimensionalize more efficiently at slightly lower R_o than the velocity and shows some degree of persistent two-dimensionalization even at very low R_o.

Finally, we display the skewness of the vorticity component parallel to the rotation axis, $S(\omega_3)$ in figure 16(*d*). A sharp maximum is observed at $R_o = 0.4$. The picture that emerges from this set of simulations is that there is a critical Rossby number around 0.1 to 0.4 where the three-dimensional modes efficiently transfer energy to the two-dimensional modes, resulting in a significant two-dimensionalization of both the velocity and vorticity. It is precisely over this range that the asymmetry between cyclones and anticyclones is maximum. Clearly the most efficient two-dimensionalization occurs via the preferential formation of cyclonic coherent vortices.

We focus on larger Rossby numbers than Mansour *et al.* (1991*a*, 1992). However,

whereas they note only a weak tendency toward two-dimensionalization at any R_o, it is significantly stronger in our work. The essential differences are the Reynolds number and the integration length. We also note considerably more two-dimensionalization in LES and hyperviscosity simulations than in the low-R_e DNS. This dependence on R_e has been studied in detail by Mansour *et al.* (1991*a*) and forms the basis of equation (1) (taken from their paper). It implies that for fixed R_o, the cascade strength is reduced at lower R_e. Our simulations show a stronger cascade rate for the three-dimensional modes than for the two-dimensional modes. A simulation must therefore be able to sustain a significant amount of downscale three-dimensional cascade, before the dissipative timescale becomes much shorter than the nonlinear timescale, in order to observe two-dimensionalization.

As the Rossby number is reduced from unity, the vorticity skewness diminishes and anticyclonic coherent structures begin to emerge provided that the Reynolds number is high enough. At extremely low R_o, the nonlinearity is greatly reduced by the inertial waves. In this régime the DNS simulations of Mansour *et al.* (1991*a*, 1992) are dominated by viscous dissipation. However, the present study suggests that at much higher R_e, such that the flow is not significantly dissipated over the nonlinear transfer timescale, a slow two-dimensionalization will occur.

5. Conclusions and discussion

These simulations have illustrated both the three-dimensionalization of initially quasi-two-dimensional flow and the two-dimensionalization of isotropic three-dimensional flow. We have observed that coherent two-dimensional eddies three-dimensionalize without rotation through the stretching of vorticity in the stagnation regions, resulting in the formation of longitudinal hairpin vortices as observed in shear flows. Their intensities eventually rival those of the initial vortices, leading to interaction and a generalized three-dimensionalization of the flow. When rotation is added, the centrifugal instability arguments predict well the three-dimensionalization of anticyclonic vortices. The subsequent evolution is best considered using the *absolute* vorticity. At maximum anticyclonic instability the Rossby number is of order one, implying that anticyclonic relative-vorticity centres have weak absolute vorticity. In §3 this weak anticyclonic vorticity was observed to be rapidly stretched out into longitudinal vortices between the stable quasi-two-dimensional cyclonic vortices. The latter were observed to persist over several tens of large-scale turnover times. For $R_o = 0.1$, on the contrary, the quasi-two-dimensional flow returned to two-dimensionality.

When simulations were started from isotropic three-dimensional initial conditions, we observed some tendency for the energy-containing scales to two-dimensionalize for $R_o \lesssim 1$. At $R_o \sim O(1)$ this occurred via the formation of coherent quasi-two-dimensional cyclonic vorticity structures typical of two-dimensional turbulence simulations. The vorticity was highly skewed with little or no intermittency in the highly three-dimensional anticyclonic regions. At $R_o = 0.1$, a few quasi-two-dimensional anticyclonic vortices were also observed to persist.

We reiterate that this study is completely consistent with previous simulations of rotating turbulence by Bardina *et al.* (1985), Dang & Roy (1985*a*, *b*), Roy (1986), Teissèdre & Dang (1987) and Mansour *et al.* (1991*a*, 1992). Whereas none of these studies noted a tendency towards anisotropy of the Reynolds tensor, most observed the anisotropy in the integral scales. The present simulations make it clear that the former occurs well after the time at which $L^u_{11,3} \approx L^u_{33,3}$, implying that previous simulations were not of sufficient duration to observe b^u_{ij} significantly different from

zero. It is perhaps not surprising that the tendency to larger vertical scales occurs before the component anisotropy. In the limit $\partial/\partial x_3 \to 0$, (2) reduces to the equations for two-dimensional turbulence in the plane perpendicular to the rotation axis. In addition, the velocity component parallel to $\boldsymbol{\Omega}$ is advected passively. Two-dimensional cascade phenomenologies show that, unlike the variance of the velocity perpendicular to $\boldsymbol{\Omega}$, u_3 (passive-scalar) variance cascades downscale to the dissipation (e.g. Lesieur 1990). This occurs on the slow timescale, τ_{NL}.

It is through our use of large-eddy simulations with two subgridscale models that we have been able to integrate longer, without the excessive viscous damping that would be present with DNS on a 64^3 grid. It is also clear from previous work that long DNS integrations at low R_e display considerably less two-dimensionalization and less vorticity coherence than our LES and hyperviscosity results. The quasi-two-dimensional coherent structures observed in simulations from isotropic three-dimensional initial conditions form and evolve nonlinearly over tens of large-scale turnover times. Whereas rapid distortion theory studies have been able to predict DNS results concerning the lack of Reynolds-stress anisotropy over short timescales, τ_L, it is hardly surprising that RDT is unable to reproduce the highly nonlinear two-dimensionalization on the slow timescale ($\sim$ tens of τ_{NL}) observed here. The vorticity asymmetry has not been extensively studied in previous work. Only Roy (1986) measured it for a low-Rossby-number simulation from quasi-two-dimensional initial conditions. In this case he observed stability of two-dimensional flow and therefore a lack of vorticity skewness. Our simulations confirm this behaviour as it is only via a three-dimensionalization that the vorticity asymmetry is manifested.

The present study might explain the rotating tank experiments of Hopfinger, Browand & Gagne (1982). Turbulence was produced by an oscillating grid oriented perpendicular to the rotation axis and located at the bottom of the tank. Whereas intense cyclonic vortices were obtained, anticyclones were found to be much weaker. In this experiment the Rossby number decreased with distance from the grid due to a simultaneous decay of turbulent kinetic energy and a growth of the integral scale. Thus, it is possible that at a distance from the grid where the local Rossby number corresponded to maximum asymmetry, cyclonic vortices were formed, as in our computations. Above, where the Rossby number was small, the flow became two-dimensional following the lower cyclonic vortices. Our explanation is proposed as an alternative to that of Mory & Caperan (1987), who drew the analogy between this experiment and thermal convection. Their study relied on the problem's inhomogeneity, with the gradient of the turbulent kinetic energy along the rotation axis playing the role of the mean temperature profile in the convection problem. This approach did not predict the observed preponderance of cyclones over anticyclones.

Our findings may also be applied to the development of intense cyclonic perturbations in the atmosphere resulting from baroclinic instability. The Rossby numbers characterizing growing perturbations may be in the range where cyclonic vorticity is favoured, although clearly the influence of density stratification must be considered. Note that Jupiter's great red spot, which is anticyclonic, has a local Rossby number much less than one, implying that rotation is two-dimensionally stabilizing. This could be a factor for the persistence of this vortex, even in a non-shallow layer.

The authors benefitted considerably from numerous informal discussions with J. J. Riley, D. J. Tritton, S. Yanase, C. Flores, B. Legras, N. N. Mansour, Y. Gagne, P. Comte, T. Warn and from the referees comments. We are also indebted to Y. Fouillet for developing the visualization software (FLOSIAN). P. B. would like to

acknowledge financial support in the form of a post-doctoral fellowship from the Natural Sciences and Engineering Research Council of Canada. The calculations were performed under a grant from the Centre de Calcul Vectoriel pour la Recherche, Palaiseau, France.

REFERENCES

ANDRÉ, J. C. & LESIEUR, M. 1977 Influence of helicity on high Reynolds number isotropic turbulence. *J. Fluid Mech.* **81**, 187–207.

ANSELMET, F., GAGNE, Y., HOPFINGER, E. J. & ANTONIA, R. A. 1984 High-order velocity structure functions in turbulent shear flows. *J. Fluid Mech.* **140**, 63–89.

BARDINA, J., FERZIGER, J. H. & ROGALLO, R. S. 1985 Effect of rotation on isotropic turbulence: computation and modelling. *J. Fluid Mech.* **154**, 321–336.

BASDEVANT, C., LEGRAS, B., SADOURNY, R. & BÉLAND, M. 1981 A study of barotropic model flows: Intermittency, waves and predictability. *J. Atmos. Sci.* **38**, 2305–2326.

BASDEVANT, C. & SADOURNY, R. 1983 Modélisation des échelles virtuelles dans la simulation numérique des écoulements turbulents bidimensionels. *J. Mec. Theor. Appl., Numéro Spécial*, 243–269.

BIDOKHTI, A. A. & TRITTON, D. J. 1992 The structure of a turbulent free shear layer in a rotating fluid. *J. Fluid Mech.* **241**, 469–502.

BRADSHAW, P. 1969 The analogy between streamline curvature and buoyancy in turbulent shear flow. *J. Fluid Mech.* **36**, 177–191.

CAMBON, C. & JACQUIN, L. 1989 Spectral approach to non-isotropic turbulence subjected to rotation. *J. Fluid Mech.* **202**, 295–317.

CHOLLET, J.-P. & LESIEUR, M. 1981 Parameterization of small scales of three-dimensional isotropic turbulence utilizing spectral closures. *J. Atmos. Sci.* **38**, 2747–2757.

COMTE, P., LESIEUR, M. & LAMBALLAIS, E. 1992 Large- and small-scale stirring of vorticity and a passive scalar in a three-dimensional temporal mixing layer. *Phys. Fluids* A **4**, 2761–2778.

DANG, K. & ROY, P. 1985*a* Numerical simulation of homogeneous turbulence. In *Proc. Workshop on Macroscopic Modelling of Turbulent Flows and Fluid Mixtures*. Springer.

DANG, K. & ROY, P. 1985*b* Direct and large eddy simulation of homogeneous turbulence submitted to solid body rotation. In *Proc. 5th Symp. on Turbulent Shear Flows*. Springer.

DRAZIN, P. G. & REID, W. H. 1981 *Hydrodynamic Stability*. Cambridge University Press.

FLORES, C. 1993 Étude numérique de l'influence d'une rotation sur les écoulements cisaillés libres. PhD thesis, National Polytechnic Institute, Grenoble.

FORNBERG, B. 1977 A numerical study of 2-D turbulence. *J. Comput. Phys.* **25**, 1–31.

GREENSPAN, H. P. 1969 *The Theory of Rotating Fluids*. Cambridge University Press.

HART, J. E. 1971 Instability and secondary motion in a rotating channel flow. *J. Fluid Mech.* **45**, 341–351.

HERRING, J. R. & MÉTAIS, O. 1989 Numerical experiments in forced stably stratified turbulence. *J. Fluid Mech.* **202**, 97–115.

HOLLOWAY, G. 1979 On the spectral evolution of strongly interacting waves. *Geophys. Astrophys. Fluid Dyn.* **11**, 271–287.

HOPFINGER, E. J., BROWAND, F. K. & GAGNE, Y. 1982 Turbulence and waves in a rotating tank. *J. Fluid Mech.* **125**, 505–534.

JACQUIN, L., LEUCHTER, O., CAMBON, C. & MATHIEU, J. 1990 Homogeneous turbulence in the presence of rotation. *J. Fluid Mech.* **220**, 1–52.

KLOOSTERZIEL, R. C. & VAN HEIJST, G. J. F. 1991 An experimental study of unstable barotropic vortices in a rotating fluid. *J. Fluid Mech.* **223**, 1–24.

KRISTOFFERSEN, R. & ANDERSSON, H. F. 1993 Direct simulations of low-Reynolds-number turbulent flow in a rotating channel. *J. Fluid Mech.* **256**, 163–197.

LESIEUR, M. 1990 *Turbulence in Fluids*, 2nd Edn. Martinus Nijhoff.

LESIEUR, M., YANASE, S. & MÉTAIS, O. 1991 Stabilizing and destabilizing effects of a solid-body rotation on quasi-two-dimensional shear layers. *Phys. Fluids* A **3**, 403–407.

MCWILLIAMS, J. C. 1984 The emergence of isolated coherent vortices in turbulent flow. *J. Fluid Mech.* **146**, 21–43.

MANSOUR, N. N., CAMBON, C. & SPEZIALE, C. G. 1991*a* Single point modelling of initially isotropic turbulence under uniform rotation. In *Annual Research Briefs*. Center for Turbulence Research, NASA-Ames Research Center - Stanford University.

MANSOUR, N. N., CAMBON, C. & SPEZIALE, C. G. 1992 Theoretical and computational study of rotating isotropic turbulence. In *Studies in Turbulence* (ed. T. B. Gatski, S. Sarkar & C. G. Speziale). Springer.

MANSOUR, N. N., SHIH, T.-H. & REYNOLDS, W. C. 1991*b* The effects of rotation on initially anisotropic homogeneous flows. *Phys. Fluids* A **3**, 2421–2425.

MÉTAIS, O. & LESIEUR, M. 1992 Spectral large-eddy simulation of isotropic and stably-stratified turbulence. *J. Fluid Mech.* **235**, 157–194.

MÉTAIS, O., YANASE, S., FLORES, C., BARTELLO, P. & LESIEUR, M. 1992 Reorganization of coherent vortices in shear layers under the action of solid-body rotation. In *Turbulent Shear Flows 8*, pp. 415–430. Springer.

MORY, M. & CAPERAN, P. 1987 On the genesis of quasi-steady vortices in a rotating turbulent flow. *J. Fluid Mech.* **185**, 121–136.

ORSZAG, S. A. 1971 Numerical simulation of incompressible flows within simple boundaries. I Galerkin (spectral) representations. *Stud. Appl. Maths* **50**, 293–327.

RAYLEIGH, LORD 1916 On the dynamics of revolving fluids. *Proc. R. Soc. Lond.* A **93**, 148–154.

REYNOLDS, W. C. 1989 Effects of rotation on homogeneous turbulence. In *Proc. of the Tenth Australasian Fluid Mechanics Conference*. University of Melbourne, Australia.

REYNOLDS, W.C. 1991 Towards a structure-based turbulence model. In *Studies in Turbulence* (ed. T.B. Gatski, S. Sarkar & C.G. Speziale). Springer.

ROY, PH. 1986 Simulation numérique d'un champ turbulent homogène incompressible soumis à des gradients de vitesse moyenne. Thèse de Doctorat d'État, Université de Nice.

SIGGIA, E. D. 1981 Numerical study of small scale intermittency in three-dimensional turbulence. *J. Fluid Mech.* **107**, 375–406.

SMYTH, W. D. & PELTIER, W. R. 1994 three-dimensionalization of barotropic vortices on the f-plane. *J. Fluid Mech.* in press.

TEISSÈDRE, C. & DANG, K. 1987 Anisotropic behaviour of rotating homogeneous turbulence by numerical simulation. In *Proc. AIAA 19th Fluid Dynamics, Plasma Dynamics and Lasers Conference, 1987 Honolulu, Hawaii.*

TRITTON, D. J. 1992 Stabilization and destabilization of turbulent shear flow in a rotating fluid. *J. Fluid Mech.* **241**, 503–523.

VAN ATTA, C. W. & PARK, J. 1972 Statistical self-similarity and inertial subrange turbulence. In *Statistical Models and Turbulence* (ed. M. Rosenblatt & C. W. Van Atta). Lecture Notes in Physics, vol. 12. Springer.

VINCENT, A. & MENEGUZZI, M. 1991 The spatial structure and statistical properties of homogeneous turbulence. *J. Fluid Mech.* **225**, 1–20.

WALEFFE, F. 1993 Inertial transfers in the helical decomposition. *Phys. Fluids* A **5**, 677–685.

YANASE, S., FLORES, C., MÉTAIS, O. & RILEY, J.J. 1993 Rotating free shear flows Part 1: Linear stability analysis. *Phys. Fluids* A **5**, 2725–2737.